FINAL TECHNICAL REPORT

Project Title:	**Alternate Fuel Cell Membranes for Energy Independence**
Project Period:	August 1, 2008 to May 31, 2012
Date of Report:	August 29, 2012
Recipient:	The University of Southern Mississippi
Award Number:	DE-FG36-08GO88106
Project Director:	Robson F. Storey
Team Members:	PIs: Robson F. Storey, Kenneth A. Mauritz Co-PIs: Derek L Patton, Daniel A Savin Post Docs: Mohammad Hassan, Andrew Jackson, Sunil Kulkarni, Haibo Li, Praveen Madasu Research Associate: Steven Suggs Graduate Students: Amol Nalawade, Nathan Kirk, Hongying Chen, Austin Baranek, Jacob Ray Undergraduate Students: William Brooks, Charles Jamison, Gregory Miller
Cost-Sharing Partners:	Denis Weisenberg, Provost
Contact:	Robson F Storey, 601-266-4849, robson.storey@usm.edu
DOE Managers:	DOE Technology Dev Manager: Dimitrios Papageorgopoulos Phone: (202) 586-5463; E-mail: dimitrios.papageorgopoulos@ee.doe.gov DOE Field Project Officer: David Peterson Phone: (720) 356-1747; E-mail: david.peterson@go.doe.gov

EXECUTIVE SUMMARY

The overall objective of this project was the development and evaluation of novel hydrocarbon fuel cell (FC) membranes that possess high temperature performance and long term chemical/mechanical durability in proton exchange membrane (PEM) fuel cells (FC). The major research theme was synthesis of aromatic hydrocarbon polymers of the poly(arylene ether sulfone) (PAES) type containing sulfonic acid groups tethered to the backbone via perfluorinated alkylene linkages and in some cases also directly attached to the phenylene groups along the backbone. Other research themes were the use of nitrogen-based heterocyclics instead of acid groups for proton conduction, which provides high temperature, low relative humidity membranes with high mechanical/thermal/chemical stability and pendant moieties that exhibit high proton conductivities in the absence of water, and synthesis of block copolymers consisting of a proton conducting block coupled to poly(perfluorinated propylene oxide) (PFPO) blocks.

Accomplishments of the project were as follows: 1) establishment of a vertically integrated program of synthesis, characterization, and evaluation of FC membranes, 2) establishment of benchmark membrane performance data based on Nafion for comparison to experimental membrane performance, 3) development of a new perfluoroalkyl sulfonate monomer, *N,N*-diisopropylethylammonium 2,2-bis(*p*-hydroxyphenyl) pentafluoropropanesulfonate (HPPS), 4) synthesis of random and block copolymer membranes from HPPS, 5) synthesis of block copolymer membranes containing high-acid-concentration hydrophilic blocks consisting of HPPS and 3,3′-disulfonate-4,4′-dichlorodiphenylsulfone (sDCDPS), 6) development of synthetic routes to aromatic polymer backbones containing pendent 1H-1,2,3-triazole moieties, 7) development of coupling strategies to create phase-separated block copolymers between hydrophilic sulfonated prepolymers and commodity polymers such as PFPO, 8) establishment of basic performance properties of experimental membranes, 9) fabrication and FC performance testing of membrane electrode assemblies (MEA) from experimental membranes, and 10) measurement of *ex situ* and *in situ* membrane durability of experimental membranes.

Although none of the experimental hydrocarbon membranes that issued from the project displayed proton conductivities that met DOE requirements, the project contributed to our basic understanding of membrane structure-property relationships in a number of key respects. An important finding of the benchmark studies is that physical degradation associated with humidity and temperature variations in the FC tend to open new fuel crossover pathways and act synergistically with chemical degradation to accelerate overall membrane degradation. Thus, for long term membrane survival and efficient fuel utilization, membranes must withstand internal stresses due to humidity and temperature changes. In this respect, rigid aromatic hydrocarbon fuel cell membranes, e.g. PAES, offer an advantage over un-modified Nafion® membranes. The benchmark studies also showed that broadband dielectric spectroscopy is a potentially powerful tool in assessing shifts in the fundamental macromolecular dynamics caused by Nafion chemical degradation, and thus, this technique is of relevance in interrogating proton exchange membrane durability in fuel cells and macromolecular dynamics as coupled to proton migration, which is of fundamental relevance in proton exchange membranes in fuel cells. A key finding from the hydrocarbon membrane synthesis effort was that rigid aromatic polymers containing isolated ion exchange groups tethered tightly to the backbone (short tether), such as HPPS, provide excellent mechanical and durability properties but do not provide sufficient conductivity, in either random or block configuration, when used as the sole ion exchange monomer. However, we continue to hypothesize that longer tethers, and tethered groups spaced more closely within the hydrophilic chain elements of the polymer, will yield highly conductive materials with excellent mechanical properties.

Another key finding is the superior performance of PAES membranes upon being subjected to open circuit voltage (OCV) testing. Throughout the course of the experiment, OCV for the PAES not only stayed higher but also decayed at a much lower rate, which is attributed to better dimensional stability and improved mechanical and gas barrier properties. The rigid backbone reinforcement of PAES adds gas diffusion tortuosity that restricts membrane degradation and OCV loss due to reduced fuel

crossover. The overall results of creep, contractile stress and mechanical tensile tests confirm the conclusion that degraded MEAs of PAES membrane can handle stress and are more likely to be more durable in a fuel cell, even after subjected to 62h of OCV degradation. Degraded Nafion MEAs were reported[1] to be unable to withstand stresses, having reduced ductility, poorer mechanical properties, and started to form cracks after 45h of OCV degradation.

COMPARISON OF ACCOMPLISHMENTS WITH GOALS AND OBJECTIVES

The overall objectives of the project were to engage in the fine molecular tailoring and evaluation of novel hydrocarbon fuel cell membranes that possess high temperature performance and long term chemical/mechanical durability in PEM fuel cells. This consisted first of establishment of standard benchmark properties of Nafion® membranes and inorganic sol-gel-modified Nafion® membranes (initial portion of Tasks 3.0, 4.0, 5.0, and 6.0). The actual accomplishments in this sub-task fully met the original goals and objectives of the project and resulted in a number of publications and presentations listed later in this report.

The next major task (Task 2.0) was the synthesis of new polymers: aromatic hydrocarbon polymers with tethered acid exchange groups (Subtask 2.1) or pendant N-heterocycles (Subtask 2.2), and PFPO-based block copolymers (Subtask 2.3). In general, accomplishments of the synthesis subtasks compared favorably with the original goals and objectives; unfortunately, none of the experimental hydrocarbon membranes that issued from the project displayed proton conductivities that met DOE requirements. A new monomer, HPPS, was developed, and random and block PAES copolymers were produced from it. None of these polymers produced the high conductivities originally hypothesized for these materials. As a result, Subtask 2.1 was re-focused on the synthesis of monomers with longer tethers and lower equivalent weight, particularly tethers derived from commercially available 5-iodooctafluoro-3-oxapentanesulfonyl fluoride. A number of attempts were made to incorporate this tether into bisphenolic monomers suitable for the synthesis of PEAS, but none were successful. Concurrently with these efforts, random and block PAES copolymers were produced using HPPS along with sDCDPS. Performance properties evaluation of these materials is ongoing and will continue even though the project funding period has ended. The primary accomplishment of Subtask 2.2 was the development of synthetic routes to achieve aromatic polymer backbones containing pendent 1H-1,2,3-triazole moieties. Triazoles are amphiprotic charge carriers, i.e., moieties capable of serving both as proton donors and proton acceptors, so water is no longer necessary as a proton transport medium. These materials provide a platform for developing a better understanding of anhydrous proton transport in glassy polymer matrices. The original objectives of Subtask 2.3 were to synthesize PFPO-poly(styrene sulfonate) (PSS) block copolymers with varying block ratios, map their phase behavior using TEM and SAXS, and quantify their water uptake and ion transport properties. Direct coupling of PS-OH and PFPO-COOH through an ester linkage was performed using carbodiimide and acid chloride approaches. This was successful but the ester linkage did not survive sulfonation of PS. Thus PFPO-COOH was fitted with terminal 4-fluorophenylsulfonyl end groups, to enable coupling with

phenolate-terminated acid-containing blocks. Coupling was successful with non-acid containing PAES but in the case of sPAES, only black, insoluble materials were obtained.

The original objectives of Task 4.0 included membrane ex situ durability characterization and MEA fabrication development. We successfully established a full spectrum of membrane ex situ durability characterization data using various techniques/methods. These techniques/methods included measurement of the following membrane characteristics: water uptake and conductivities at various humidities and temperatures, and mechanical tensile, creep, and contractile stress behaviors under fuel cell operating conditions. These tests enabled us to rapidly screen membrane mechanical durability before and after subjection to local stresses generated by variations in humidity and temperature during fuel cell testing. MEAs were successfully developed for membranes having good conductivity and mechanical durability. Broadband dielectric spectroscopy was used to assess shifts in the fundamental macromolecular dynamics caused by Nafion chemical degradation as well as interrogate its chain dynamics as coupled to proton migration. We were unable to use this technique to analyze chemical degradation and macromolecular dynamics of PAES membranes due to lack of enough quantities of materials.

Task 5.0 involved inorganic sol-gel modification and characterization of benchmark Nafion and hydrocarbons membranes. This effort was successfully completed for Nafion but was discontinued for the hydrocarbon materials.

Task 6.0 targets of fuel cell performance and membrane *in-situ* durability studies were successfully accomplished for both Nafion benchmark and PAES membranes. These studied included membranes fuel cell performance and OCV degradation tests. None of the PAES membranes prepared in this project displayed fuel cell performance that met DOE requirements. Nonetheless, one of the PAES membranes showed good mechanical durability even after subjected to 62h of OCV degradation. Mechanical durability tests, including tensile, creep, and contractile stress, were successfully conducted as planned for MEAs before and after the OCV tests.

SUMMARY OF PROJECT ACTIVITIES

Task 1.0 Acquisition of Equipment

All proposed equipment purchases were made, and all equipment is operational and actively used on a daily basis.

Task 2.0 Synthesis of Polymers

Subtask 2.1 Synthesis of Aromatic Polymers with Tethered, Acidic Ion Exchange Sites

A synthesis of the perfluoroalkyl sulfonate monomer, *N,N*-diisopropylethylammonium 2,2-bis(*p*-hydroxyphenyl) pentafluoropropanesulfonate (HPPS), in three steps from hexafluoroacetone and phenol was developed, as shown in Scheme 1.[2] Random PAES were prepared by copolymerization of varying molar ratios of HPPS/biphenol (BP) with bis(4-fluorophenyl)sulfone (FPS), as shown in Scheme 2.2 The random copolymers are identified with their experimental compositions and molecular weight, ion exchange capacity (IEC), and conductivity data in Table 1.2

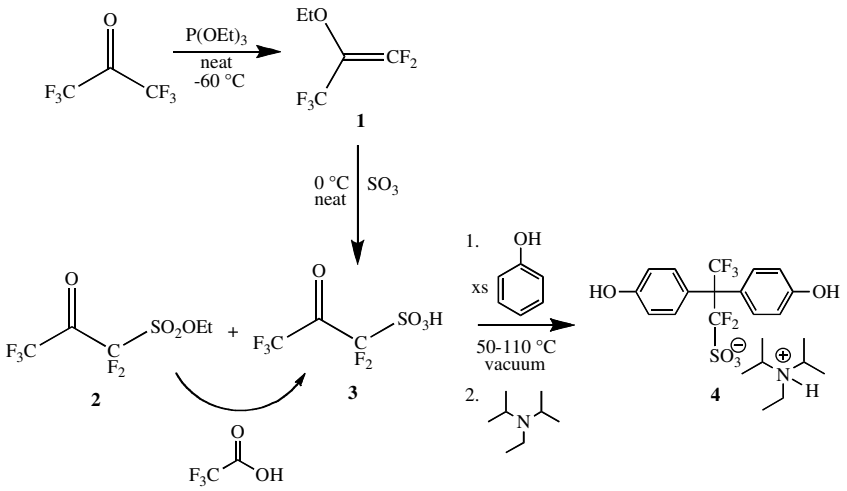

Scheme 1. Synthesis of *N,N*-diisopropylethylammonium 2,2-bis(*p*-hydroxyphenyl)penta-fluoropropanesulfonate (HPPS) (**4**).

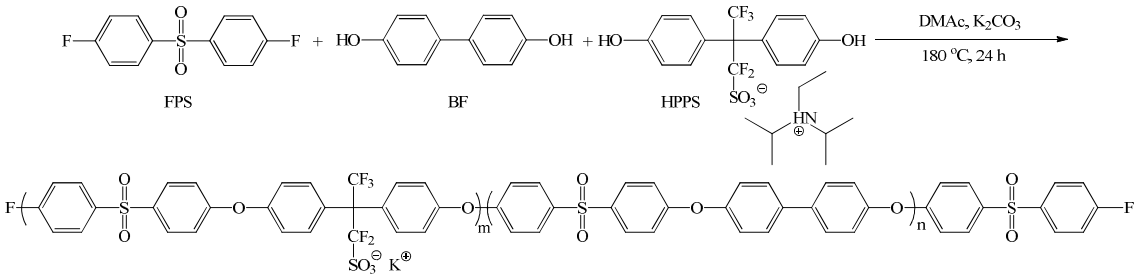

Scheme 2. Preparation of random poly(arylene ether sulfone) (PAES) from HPPS, BF, and FPS.

Table 1. Composition and Molecular Weights of Random Copolymers from HPPS, BP, and FPS

Copolymer[a]	Composition (theo)[b]	$M_{n,theo}$ (g/mol)	$M_{n,NMR}$ (g/mol)	$M_{n,GPC}$ (g/mol)	M_w/M_n (GPC)	IEC[c] (meq/g)	Conduct. (mS/cm)
PAES-20	20/80	25,000	27,100	28,400	1.63	0.36	1.6
PAES-31[d]	30/70	33,700	31,900	27,500	1.76	0.63	1.4
PAES-40	40/60	29,100	27,800	38,700	1.63	0.84	2.5
PAES-49	50/50	32,200	31,400	33,700	1.88	1.08	21
PAES-61	60/40	35,900	28,500	29,900	2.11	1.25	23

[a] The number (20, 31, 40, 49, 61) represents the value of m/(m+n) determined experimentally by ^{1}H NMR (m and n defined in Scheme 2).
[b] From comonomer feed ratios.
[c] From titration.
[d] This sample is the same as R(HPS-BP)_1,590 in Table 4.

Multi-block PAES copolymers containing HPPS were also prepared, using a two-prepolylmer approach, as shown in Scheme 3.[3] Hydrophilic prepolymers carrying 4-fluorophenyl sulfonyl end groups were synthesized by reaction of HPPS with excess FPS,

and hydrophobic prepolymers carrying potassium phenolate end groups were prepared from FPS and excess BP. The prepolymers were reacted at a theoretical 1:1 (mol:mol) fluorophenyl:potassium phenolate stoichiometry at 180°C in *N*,*N*-dimethylacetamide in the presence of K_2CO_3, for only 80 min to minimize transetherification. The resulting multi-block copolymers are identified with their experimental compositions and molecular weight, ion exchange capacity (IEC), and conductivity data in Table 2.

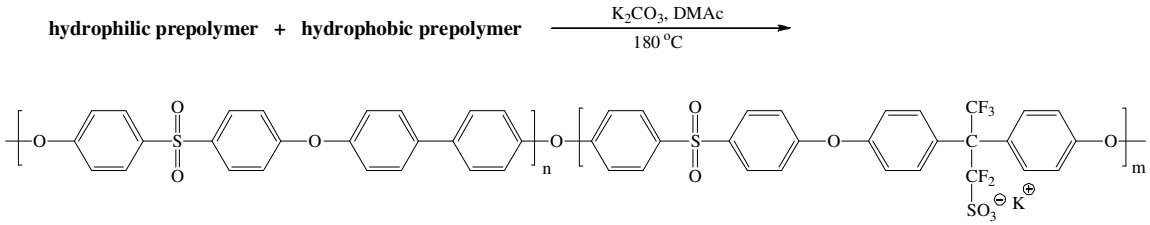

Scheme 3. Preparation of multi-block PAES copolymers containing HPPS.

Table 2. Composition and Molecular Weights of Multi-Block Copolymers from HPPS, BP, and FPS

Multi-Block Copolymer	Block Length Ratio (exp)[a]	$M_{n,GPC}$ (g/mol)	M_w/M_n (GPC)	IEC[b] (meq/g)	Conductivity (mS/cm)
HLMB-1	9.4/4.4	47,700	2.61	0.99±0.01	12.7±2.1
HLMB-2[c]	13.3/6.0	84,300	3.83	1.17±0.04	34.3±1.5
HLMB-3	16.1/8.2	81,300	2.81	1.34±0.12	14.3±2.5
HLMB-4	23.4/11.8	55,100	2.53	1.30±0.18	6.2±0.7

[a] m/n, Scheme 3, determined experimentally by ^{13}C NMR.
[b] From titration.
[c] This sample is the same as MB(HPPS-BP)_784 in Table 4.

PAES multi-block copolymers with hydrophilic blocks composed of HPPS and sDCDPS were prepared using a two stage reaction sequence (one-prepolymer method), as shown in Scheme 4. In Stage 1, the monomers BP and 4,4′-dichlorodiphenylsulfone (DCDPS) were used to synthesize phenoxide-terminated hydrophobic prepolymers in the range of 5,000 -15,000 g/mol. HPPS and sDCDPS were then added to the reaction to increase the molecular weight and incorporate hydrophilic sequences in the polymer (Stage 2). Two block copolymers of this type were prepared, designated MB (HPPS-sDCDPS)_595 and MB (HPPS-sDCDPS)_917. Table 3 lists ion exchange capacity (IEC), conductivity, molecular weight (GPC), and composition of these two materials.

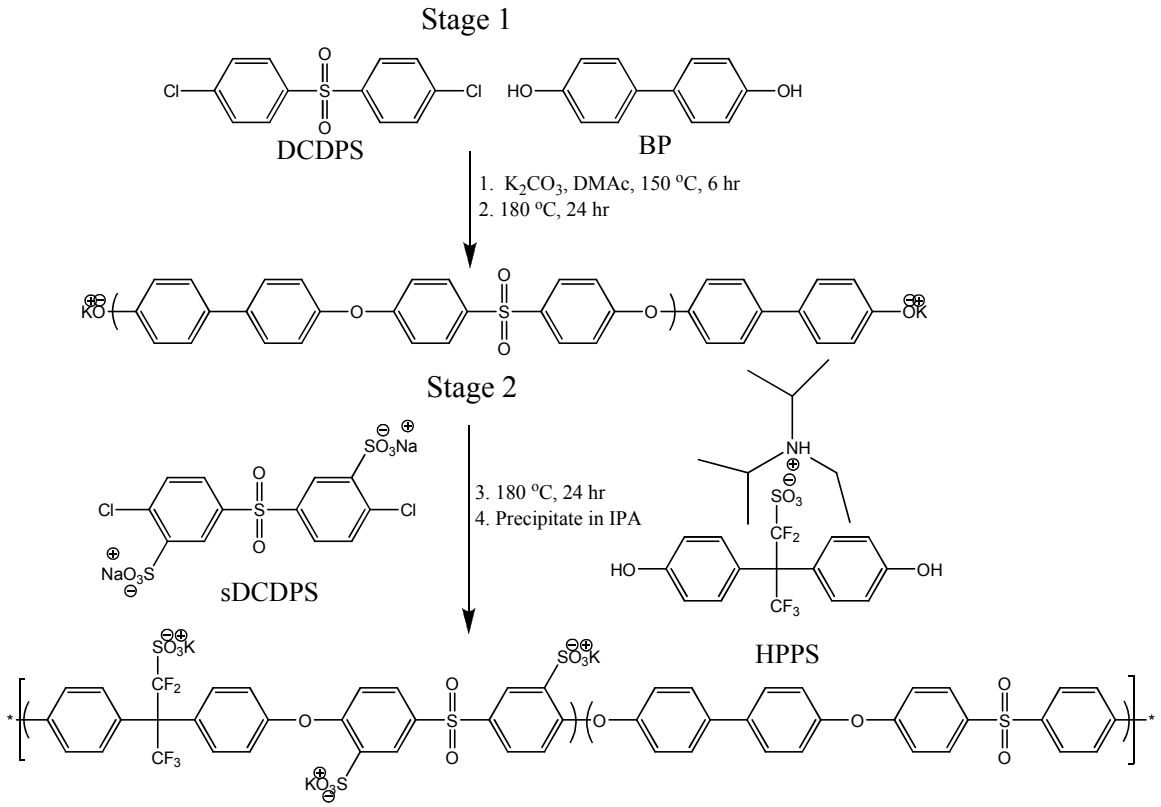

Scheme 4. Preparation of multi-block PAES copolymers containing HPPS and sDCDPS.

Table 3. Characterization Data for Multi-Block sPAES Copolymers with Hydrophilic Blocks Composed of HPPS and sDCDPS

Multi-block sPAES	IEC (meq/g)	Conductivity mS/cm	M_n (g/mol)	M_w (g/mol)	wt% hydrophilic block
MB (HPPS-sDCDPS)_595	1.68	49.9	18,550	27,330	23
MB (HPPS-sDCDPS)_917	1.08	2.2	25,120	35,170	49

Subtask 2.2 Synthesis of Pendant N-heterocycle Aromatic Main-chain Polymers

Pendant N-heterocycle aromatic polymers were prepared by grafting 1H-1,2,3-triazole-containing moieties onto a commercially available polysulfone (PSf) backbone. An *N*-protected triazole moiety, synthesized through copper-catalyzed 1,3-dipolar cycloaddition of propargyl alcohol with azidomethyl pivalate, was reacted with 4-bromophenol (Mitsonobu reaction) to afford a 4-bromophenol functionalized triazole, as shown in Scheme 5. This was followed by C-H activation and Suzuki-Miyaura coupling of the triazole moiety onto the PSf backbone, followed by deprotection as shown in Scheme 6.

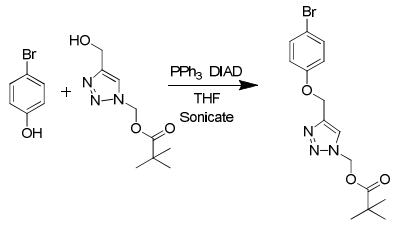

Scheme 5. Mitsonobu reaction with 4-bromophenol and the N-protected triazole to afford the 4-bromophenol functionalized triazole.

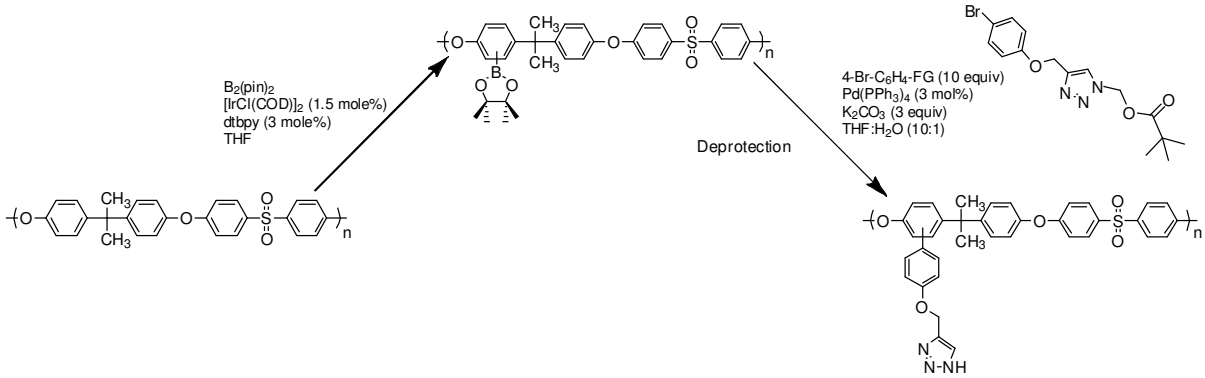

Scheme 6. Functionalization of aromatic rings of polysulfone through C-H activation and Suzuki-Miyaura reaction followed by deprotection under basic conditions.

However, the glassy nature of the PSf matrix limits the mobility of the triazoles and decreases the charge transport capabilities even at a high concentration of triazoles, i.e. one triazole per repeat unit. The high glass transition temperature of the backbone also limits the ability of the material to undergo phase separation to create continuous channels for the proton conduction. Thus, longer triazole tethers were synthesized in attempt to improve the mobility of the pendent triazoles. First, an asymmetric addition of propargyl bromide across hexane diol was carried out followed by a copper-catalyzed 1,3-dipolar cycloaddition with azidomethyl pivalate to give the terminal *N*-protected triazole alcohol (Scheme 7). Lastly, a Mitsunobu etherification with 4-bromophenol provided the 4-bromophenol functionalized triazole. However, PSf materials functionalized with triazoles on a longer tether still showed no appreciable conductivity. The low conductivity was presumably due to immobilization of a relatively low concentration of triazole within the glassy PSf matrix.

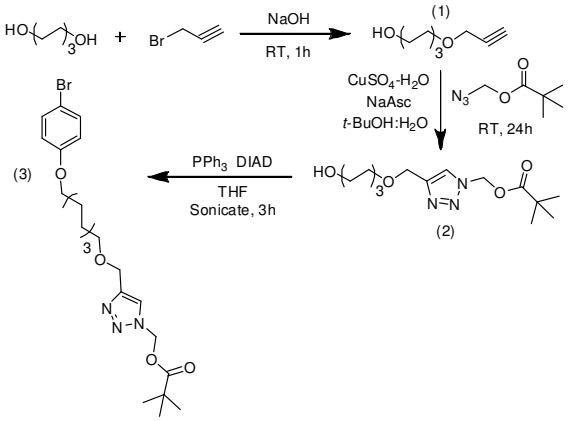

Scheme 7. Asymmetric addition of propargyl bromide across hexane diol to give (1); copper-catalyzed 1,3-dipolar cycloaddition of (1) with azidomethyl pivalate to give the terminal *N*-protected triazole alcohol (2); Mitsunobu etherification between (2) and 4-bromophenol to yield the completed tether intermediate (3).

To address the issues encountered with low conductivity of the 1H-1,2,3-triazole tethered PSf materials, we adopted a grafting from approach to enable the incorporation of a higher concentration of triazole into the PSf matrix. First, chloromethylated PSf with degrees of chloromethylation ranging from 0.25-1.9 (i.e. chloromethyl groups per repeat unit) were synthesized using a standard literature procedure.[4] As a model reaction, MMA was then grafted from the chloromethylated PSf using atom transfer radical polymerization (ATRP) conditions. The average degree of polymerization (DP) from the chloromethalated PSf backbone was around five MMA units per PSf repeat unit for all trials; however a large fraction of the chloromethyl groups remained after polymerization. This indicated an inefficient initiation process and/or a high degree of termination across the chloromethylated PSf macroinitiator. Further investigation into the ATRP grafting from approach will be necessary to optimize the reaction conditions to achieve higher initiation efficiencies.

Subtask 2.3 Synthesis and Phase Behavior of PFPO-based Block Copolymers

The overall objectives of Subtask 2.3 were to synthesize proton conducting, phase-separated block copolymers, whereby we could (1) map out the phase behavior of various molecular weight block copolymers and (2) relate morphology to performance as fuel cell membranes. The challenges here were to determine proper solvent/solvent mixtures, reaction temperatures, concentrations, etc., to effectively produce block copolymers. Initially, the work was centered around establishing efficient coupling strategies of acid chloride-functional PFPO with hydroxyl-functional poly(styrene) (Scheme 8). Here, we used dynamic light scattering (DLS) to confirm successful reactions between PS and PFPO as well as to determine changes in aggregation after sulfonation to yield sulfonated-PS-PFPO (sSF) (Figure 1). The uniform, large aggregate size in THF (a selective solvent for the styrene block) illustrates efficient synthesis of SF block copolymers without the presence of homopolymer impurities. However, after sulfonation, the aggregate sizes are extremely small with radius values around sizes that might be anticipated for unimers; this suggests that scission is possibly occurring between

PS and PFPO which seems to be a likely occurrence since the two blocks are connected by an ester linkage (susceptible to hydrolysis). Figure 2 presents an AFM phase image for SF 5-4 (where the 5 and 4 correspond to 5K PS polymer and 4K PFPO.) Our hypothesis was that by creating nano-phase separated membranes, proton conduction would be optimized by yielding well-defined channels of transport. This image suggests the expected lamellar formation with domain sizes of approximately 10 nm. Further work was devoted to creating phase-separated films of sSF block copolymers; however, it was found that the sulfonated block copolymers were highly brittle (likely due to the low molecular weight) and insufficient for making a stable film. At this point, we used our knowledge base of reaction conditions to couple the PFPO to mechanically robust proton conducting polymers made by the Storey research group, whereby the linkage between the two blocks would be one of high stability to temperature and moisture.

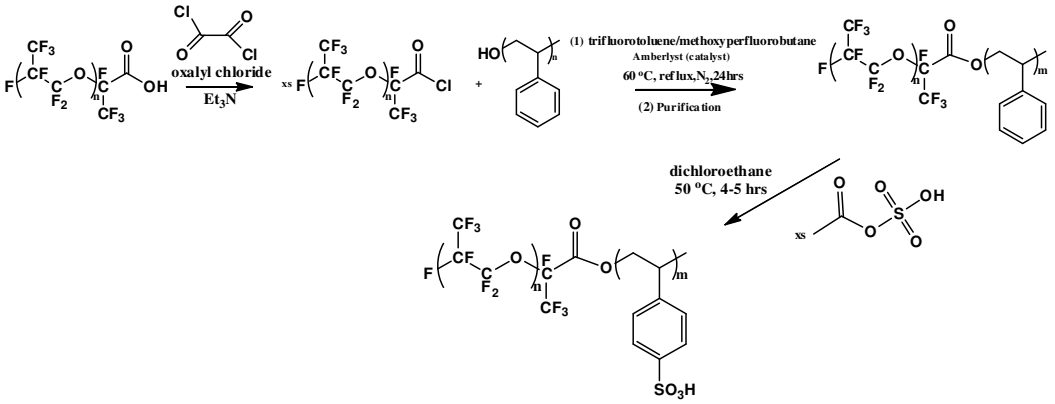

Scheme 8. Complete proposed synthesis of SF and sSF block copolymers.

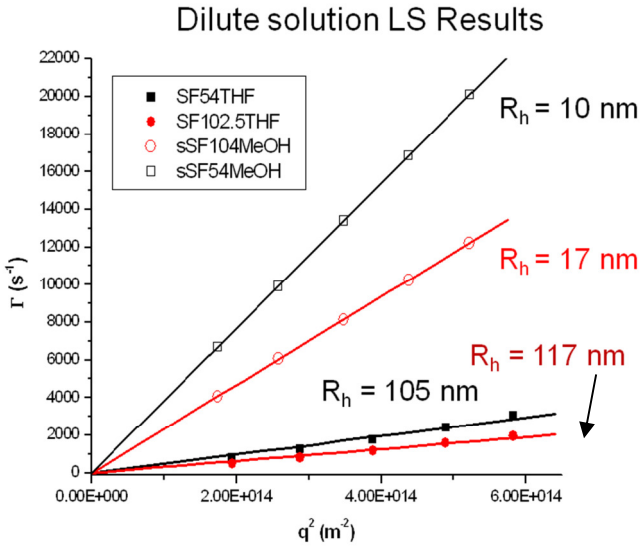

Figure 1. Dilute solution DLS results for PS-b-PF (SF) block copolymers and PSS-b-PFPO (sSF) (post-sulfonation).

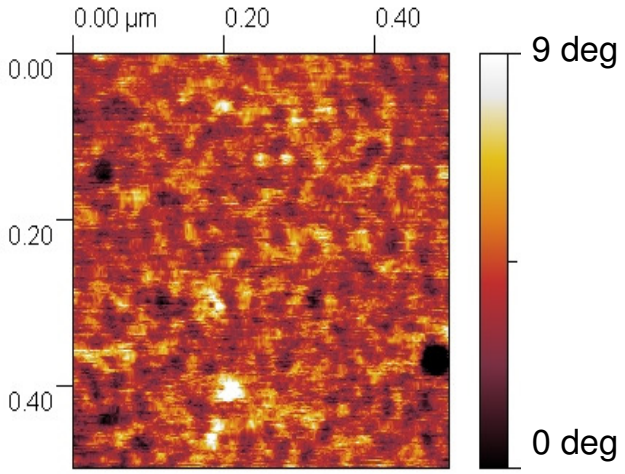

Figure 2. AFM phase image of a 50 mg/mL $PFPO_{4K}$-PS_{5K} spin-cast from a solution of 80% trifluorotoluene and 20% methoxynonafluorobutane.

Further work consisted of modifying the functionality of PFPO-COOH to facilitate efficient coupling with proton-conducting blocks, particularly hydroxyl-functional poly(aryl ether sulfone) (PAES) to yield high strength block copolymers with stable, robust linkages. PFPO chain end modification was performed by reacting PFPO-COOH with diamino halide compounds to form benzimidazole groups (Scheme 9a and 9b). In Scheme 9a the benzimidazole is formed with fluorine and bromine substituents at the 4-position on the benzene ring. In the case of fluorine, direct nucleophilic aromatic substitution (NAS) coupling reactions with hydroxyl-terminated PAES may be possible; however, due to the electron donating character of the amino groups, this is a higher energy reaction leading to insufficient coupling. Thus, we performed a second reaction on the bromine-substituted PFPO-benzamidazole to yield a compound with a strongly electron withdrawing sulfonyl group para to the fluorine, thereby activating the benzene ring for NAS (Scheme 9b). Additional work was done with the fluorine-substituted PFPO-benzimidazole (PFPO-bzimF) shown in Scheme 9a, which produced a significant color change from brown to a dark indigo; furthermore, ^{1}H NMR confirmed the presence of the aromatic protons associated with the benzimidazole. Since ^{1}H NMR suggested a successful reaction, we attempted NAS coupling with hydroxyl-terminated PAES. Encouragingly, we were able to make a homogenous solution in hexafluoroisopropanol (HFIP), and the reaction was allowed to react for 1 day at 120°C. Dynamic light scattering (DLS) results of the reaction product of PFPO-$bzimF_{2.5K}$ and $PAES_{5K}$ are shown in Figure X4. The linearity in the Γ vs. q^2 plot indicates the presence of self-assembled particles of uniform size (calculated R_h = 45 nm). However, the successful reaction was between PFPO-bzimF and non-sulfonated, hydrophobic PAES. Multiblock PAES systems composed of sulfonated and non-sulfonated blocks PAES (synthesized by the Storey and Mauritz research groups) were found to be insoluble in HFIP, which created a need for another solvent/solvent mixture for reaction with PFPO-bzimF. We had been investigating solvent systems that would be appropriate for reactions of PFPO-bzimF with proton-conducting multi-block PAES systems. The Storey group has currently synthesized several PAES multiblock systems with varying compositions of

sulfonated and non-sulfonated blocks. The goal here is to incorporate the highest content of sulfonated blocks without compromising the physical properties (i.e. brittle films). At the end of this project, we had been attempting to end-cap these systems with PFPO blocks, possibly increasing the ductility and toughness of the films while allowing for the production of organized nanophase-separated film morphologies.

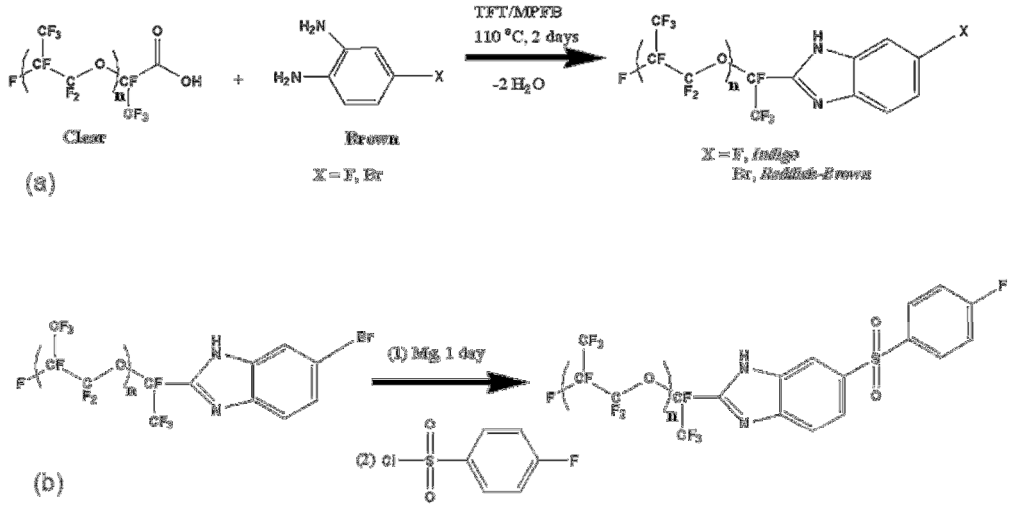

Scheme 9. Benzamidazole functionalization of PFPO-COOH to yield reactive moieties for NAS.

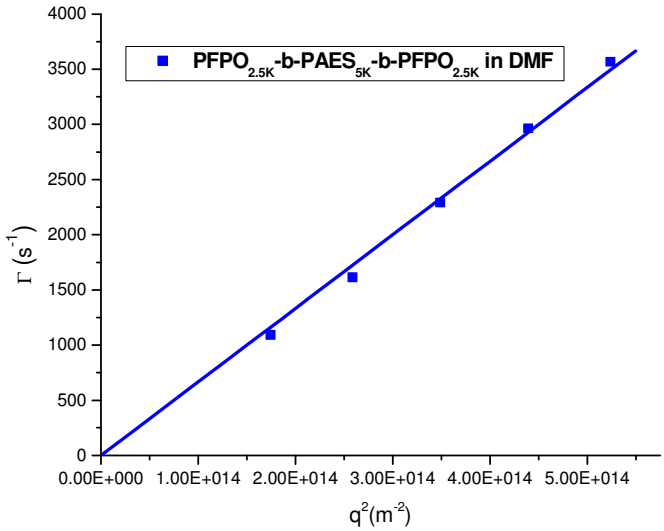

Figure 3. Γ vs. q^2 plot from DLS for a PFPO-b-PAES-b-PFPO triblock copolymer in DMF. The size (45 nm) is indicative of self-assembly from the insolubility of the PFPO blocks in DMF.

Task 3.0 Establishment of Standard Membrane Benchmark Data

Nafion®. The reader is referred to Subtask 4.1 and 4.2 and Tasks 5.0 and 6.0. These sections summarize our most important findings regarding benchmark Nafion® performance properties as films and MEAs.

Hydrocarbon. A random copolymer of sDCDPS and BP, R(sDCDPS-BP)_654, was prepared according to published procedures,[5] to serve as a standard hydrocarbon membrane against which our experimental hydrocarbon membranes could be compared. All of the ex situ membrane performance tests, mechanical durability tests, etc., found in Subtasks 4.1 and 4.2 contain comparisons to this control polymer.

Task 4.0 Membrane Characterization and MEA Fabrication

Nafion®. The reader is referred to Subtask 4.1 and 4.2.

Hydrocarbon. Shown in Table 4 are molecular weight, equivalent weight (EW), conductivity, and relevant mechanical performance data for several multi-block (MB) and random (R) copolymer samples synthesized in the project. The syntheses of these MB and R copolymers have been described in an earlier section of the report (Subtask 2.1); their chemical structures are shown in Figure 4.

Table 4. Composition and Performance Data for Various PAES Copolymers Incorporating sDCDPS and/or HPPS Monomer Units

Sample	M_n (g/mol)	M_w/M_n	Eq. Wt. (g/mol)	Conductivity (mS/cm)[a]	Stress-strain*		
					Modulus (MPa)	Stress @ Break (MPa)	Strain @ Break (mm/mm)
MB (HPPS-sDCDPS) 917	25,120	1.40	917	2.2	897.2	48.7	0.31
MB (HPPS-sDCDPS) 595	18,550	1.47	595	49.9	221.2	19.3	0.24
R (HPPS-BP) 1,260	45,800	2.89	1,260	5.7	328.1	32.5	2.15
R (HPPS-BP)_1,590[b]	27,500	1.76	1,590	1.4	-	-	-
MB (HPPS-BP)_784[c]	84,300	3.83	784	35.9	110.7	16.2	0.099
R (sDCDPS-BP) 654	14,100	1.42	654	88.5	57.6	5.9	0.108

[a] Conductivity and stress-strain measurements were conducted at 80°C and 100% RH.

[b] This sample is the same as PAES-31 in Table 1.

[c] This sample is the same as HLMB-2 in Table 2.

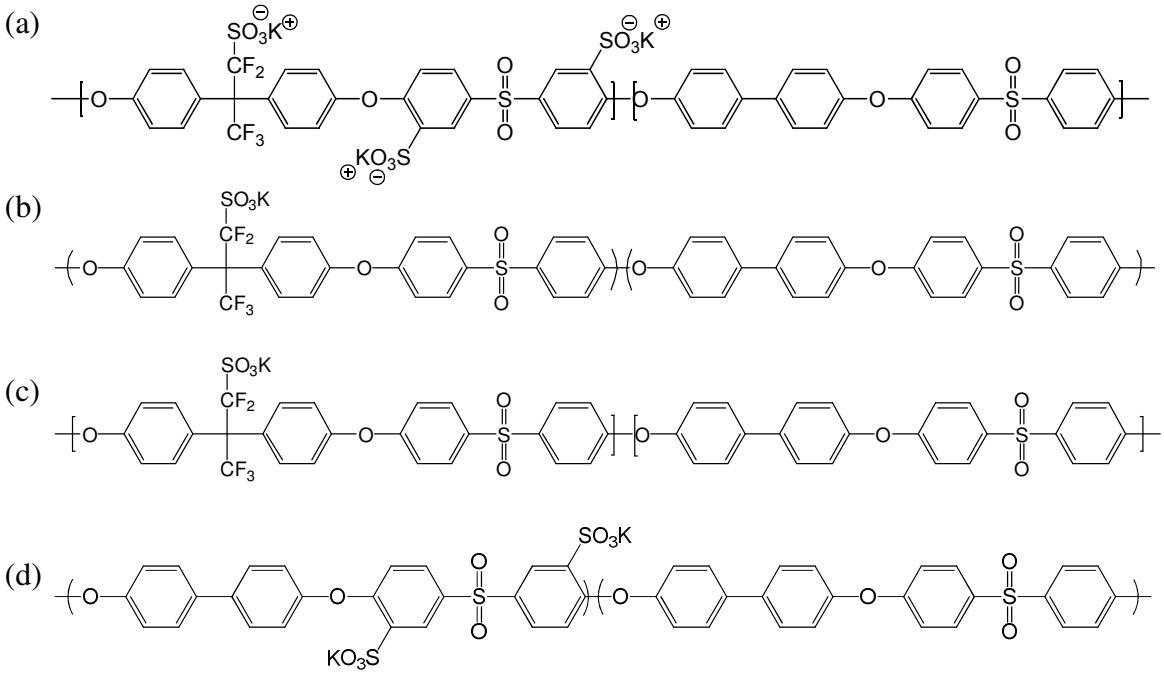

Figure 4. Chemical structures of the various polymer types in Table 4: (a) MB(HPPS-sDCDPS); (b) R(HPPS-BP); (c) M(HPPS-BP); (d) R(sDCDPS-BP).

Equilibrium water uptake of the copolymers, at 80°C over a range of relative humidity (RH), was measured using a TA Q5000SA moisture analyzer. Samples were subjected to a drying step for 100 min, then an isothermal desorption was established. The samples were examined over the range of 90-0% RH by decreasing the humidity 10% and allowing the sample to equilibrate for 1 h. Water desorption curves for copolymers with different compositions are shown in Figure 5.

The water uptake results showed that MB copolymers composed of hydrophilic blocks containing both HPPS and sDCDPS, MB(HPPS-sDCDPS) (Figure 4a) displayed the expected trend of increasing water absorption with decreasing equivalent weight. Comparing both conductivity and water uptake results for the MB(HPPS-sDCDPS)_595 and MB(HPPS-DCDPS)_784 samples suggests that incorporation of both HPPS and sDCDPS in the hydrophilic block will improve the conductivity of our membranes without increasing water uptake. More testing is being conducted to confirm our results; however the MB(HPPS-sDCDPS)_595 membrane exhibited a conductivity of 49.9 mS/cm at 100% RH. The data obtained from water activity and conductivity measurements, for the MB(HPPS-sDCDPS)_595 sample, suggest improved performance of the copolymer due to decreased isolation of hydrophilic domains, which allows achievement of higher conductivity without influencing water uptake. The improvement in morphology allows better conductivity without the need for more water, which is beneficial from a swelling/durability standpoint and will be discussed in detail later in this report. It is expected that improvements in the synthesis of these MBs, such as improved molecular weight and block length, would lead to further enhancement of their conductivity and mechanical strength.

The random copolymer containing only sDCDPS as ion-exchange comonomer, R(sDCDPS-BP)_654, achieved the highest conductivity among our samples, at 100% RH and 80°C, but also showed highest water uptake which we have found to significantly affect the mechanical durability.

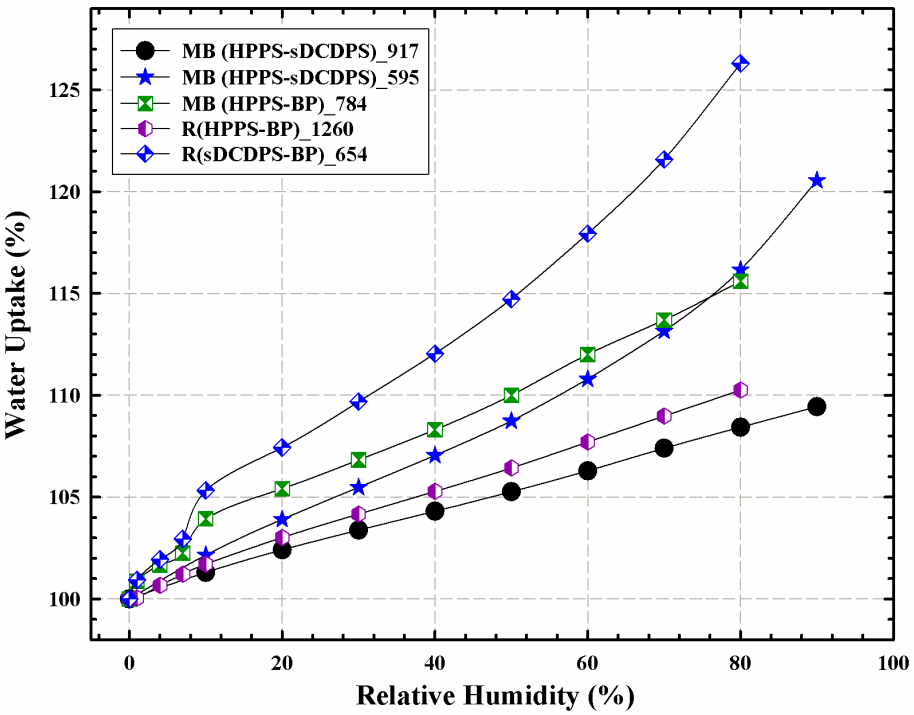

Figure 5. Water uptake vs. relative humidity at 80°C of the various samples listed in Table 4.

Subtask 4.1 Membrane *ex Situ* Durability Characterization

Nafion®. In a series of studies, broadband dielectric spectroscopy was used to probe the dynamics of macromolecular motions as coupled to proton migration within Nafion® membranes upon exposure to stimuli, e.g., annealing at high temperature and low RH, chemical degradation, etc., intended to simulate the harsh conditions within a fuel cell.[6,7,8] These fundamental molecular processes are of interest at temperatures above 100°C; in particular, spectral changes were investigated in real-time at 140°C. Loss permittivity vs. frequency spectra of both β and α relaxations showed increased relaxation times with annealing and that water de-sorption and diminished free volume were mainly responsible for these behaviors. Spectra were analyzed using the Havriliak-Negami equation and relaxation/conductivity parameters were obtained from equation fitting to experimental data to understand the nature and coupling of conduction and relaxations as annealing progressed in the instrument. A parameter *N*, reflecting the connectedness of charge hopping pathways, indicated tortuous random pathways. As *N* decreased with increased annealing time, the conductivity network appeared to accumulate more charge traps, presumably due to free volume decrease, with increased annealing time. Conductivity increased with increased annealing time at all temperatures despite the decrease in *N*; this suggests a change in the nature of proton hopping on

annealing at high temperatures to be between sulfonic acid groups rather than by hopping across H_2OH^+-OH_2 bonds.

When broadband dielectric spectroscopy was used to probe changes in macromolecular dynamics of Nafion® as a result of chemical degradation, particularly those associated with the T_g-related β relaxation, loss permittivity vs. frequency spectra showed peak splitting reflecting microstructural heterogeneity. Spectra were analyzed using the conductivity-modified Havriliak-Negami equation and the Kramers-Krönig integral transform, both of which showed broadening and peak splitting for degraded samples. Peak broadening and bi and tri-modal character of the spectra of degraded samples was also manifest in distributions of relaxation times which reflected a broadening of molecular weight distribution and related microstructural heterogeneity induced by chemical degradation.

Hydrocarbon. *Mechanical Durability.* Fuel cell membranes experience different degrees of hydration caused by humidity and temperature variations during fuel cell operation under conditions of start–stop and changes in current density.[9] These variations across mechanically constrained membrane–electrode assemblies (MEAs) cause differential swelling, thereby creating internal stresses that result in membrane deformation and failure. This was shown by relative humidity (RH) cycling tests, whereby Nafion® MEAs formed cracks due to reduced ductility.[10] Poor dimensional stability not only weakens membranes but creates pathways for fuel crossover that form hydrogen peroxide due to incomplete reduction of oxygen on the catalyst surface. Aoki et al. showed that for membrane degradation, hydrogen, oxygen, and platinum are necessary[11] suggesting this process can occur anywhere at the cathode, anode or inside the membrane where platinum bands are formed.

Physical and chemical degradations are coupled processes. In a hydrated fuel cell the phase separated, inter-connected ionic clusters offer the path of least resistance to gas diffusion as compared to the more tightly packed crystalline regions. In addition, the membrane structure expands after hydration, creating easy pathways for fuel gas to migrate to opposite electrodes. During fuel cell operation these regions continuously weaken due to reduced ductility and decreasing average polymer molecular weight, creating larger defects. The situation is analogous to environmental stress cracking wherein the reactive environment in this case contains •OH radicals and the membrane undergoes stress due to humidity changes in an operating fuel cell. This degradation process will continue until the affected regions eventually form pinholes, resulting in ultimate failure.[12]

To characterize the resistance of our hydrocarbon membranes to these physical and chemical degradation processes, we performed various mechanical tests to compare the mechanical durability of the several MB and R copolymers listed in Table 4, at operating fuel cells conditions. These tests reveal the importance of membrane mechanical properties and correlate how deterioration in mechanical properties results in chemical degradation that can lead to failure initiation in these membranes.

Tensile properties under typical fuel cell operating conditions were measured using an MTS Alliance RT/10 tensile setup equipped with a 100N load cell. A custom-designed environmental chamber and sparger were built to control chamber temperature and humidity. The membranes, after being clamped in the chamber, were conditioned for 2 h with a 100% RH nitrogen stream at a flow rate of 300 mL/min and a temperature of

80°C. Samples were then stretched at a rate of 10 mm/min. Figure 6 shows the initial strain region of the stress-strain curves for all samples at 100% RH and 80°C. Curves are displaced rightward along the strain axis, to different extents, because of dimensional increase due to water uptake. This is not the case for the MB (HPPS-sDCDPS)_917 sample, which indicates low water uptake and higher dimensional stability for this sample compared to all the others. After this stress lag, the curves for all samples, shown in Figure 7, are "typical" and a modulus can be computed from the initial, displaced linear regions. Mechanical parameters extracted from curves in Figure 7 are shown in Table 4. Generally, membranes with high conductivities suffered failure at low strain and displayed reduced ductility compared to those with lower conductivities, except for the MB(HPPS-sDCDPS)_595 sample, which exhibited moderate mechanical behavior intermediate between the two categories. A sample with a lower modulus is predicted to be easily deformed when subjected to stresses and to more easily rupture due to reduced stress-at-break, thereby promoting pathways for fuel crossover that lead to membrane failure. The correlation between mechanical durability and fuel cell performance cannot be fully established until we perform in-situ open circuit voltage tests for all membranes and compare the results to that of the benchmark Nafion or R(sDCDPS-BP)_654. Considerably lower strain-at-break for some samples in Figure 7 is presumably due to decreased molecular weight compared to that of R(HPPS-BP)_1260, since short chains can easily slip through entanglements, or may be too short for entanglements to form at all, and thus are unable to resist deformation. This value is also likely to be affected by the degree to which the samples absorbed water, which results in swelling and plasticization of the membranes.

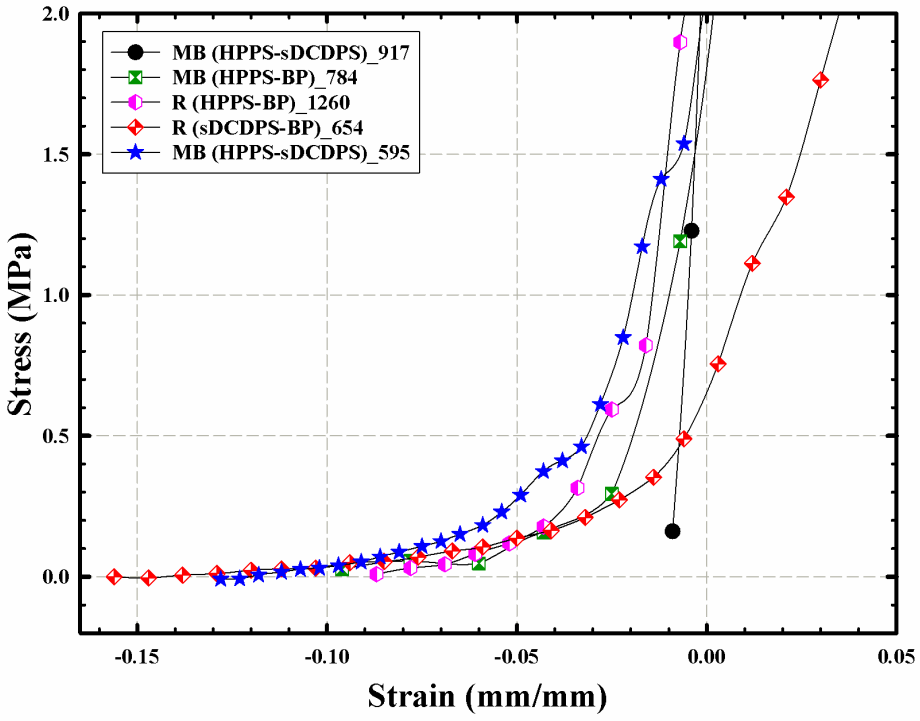

Figure 6. Initial strain region of the stress-strain curves for sPAES samples with different composition at 100% RH and 80°C.

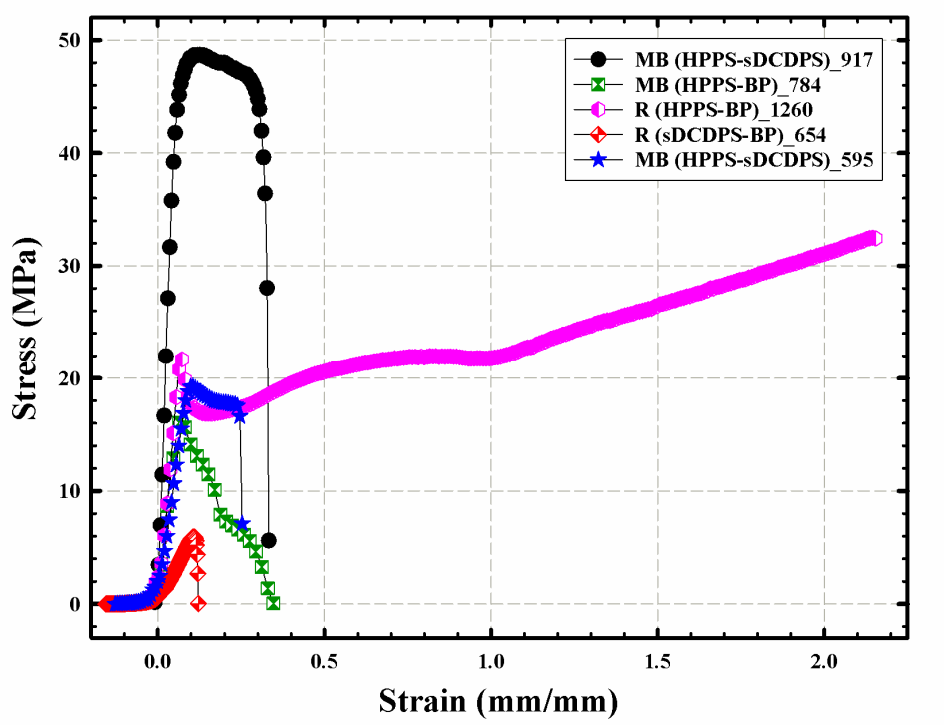

Figure 7. Stress-strain curves for sPAES samples with different composition at 100% RH and 80° C.

Contractile Stress Test. Contractile stresses generated by the membranes upon shrinkage when subjected to a drop in RH, were monitored under the same conditions used in the tensile studies. However, in this test, samples were held at their extended swollen length by zeroing the load cell and slowly adjusting the crosshead position until a tension of 0.4N was reached. The crosshead position was then locked, and the 100% RH nitrogen stream was switched to dry nitrogen at the same flow rate while maintaining the temperature of the dry stream and chamber temperature at 80°C.[12] This change of circulating gas causes the membrane to dry and attempt to contract. The ensuing contractile force is then monitored as a function of time. The stress levels developed are diagnostic of the ability of the membrane to resist dimensional changes associated with drying and are related to mechanical durability. The stress–time profiles for the membranes showed peaks at different times with the sPAES exhibiting higher stress than Nafion®, Figure 8.

In the sPAES samples, stress initially drops below zero due to drying of the chamber. During the first 60 min of drying, some of the samples started to show a slight initial increase in stress, e.g., R(sDCDPS-BP)_654, R(HPPS-BP)_1260 and MB(HPPS-sDCDPS)_595. After ≅ 50 to 80 min, all samples started to show a large increase in the stress, reflecting faster/excessive water drying rate. The R(sDCDPS-BP)_654 and MB(HPPS-sDCDPS)_595 samples, which have the highest conductivities, could not withstand drying times longer than 75 min after the second big stress rise. The MB(HPPS-sDCDPS)_595 sample exhibited much higher stress before failure compared

to the R(sDCDPS-BP)_654 sample. This indicates greater resistance to mechanical deformation at high temperature and humidity for the MB(HPPS-sDCDPS)_595 sample.

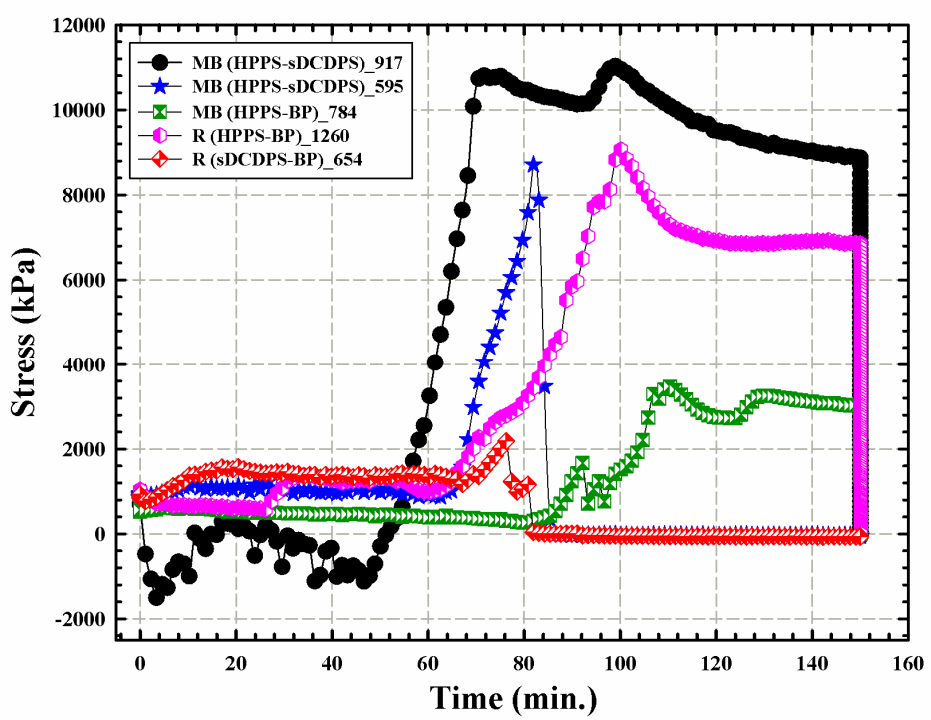

Figure 8. Contractile stress response to humidity decrease from 100 to 0% RH at 80°C for various sample listed in Table 4.

The MB(HPPS-sDCDPS)_917, MB(HPPS-BP)_784 and R(HPPS-BP)_1260 samples were able to withstand higher induced contractile stress, compared to R(sDCDPS-BP)_654 and MB(HPPS-sDCDPS)_595, and kept yielding for longer times prior to rupture, most likely due to the resistance these membranes have to macromolecular chain slippage. These samples also suffered from non-catastrophic crazes as indicated by the stress drop/rise events shown in Figure 8. Previously it was determined that the second stress increase in Nafion® must be due to a longer range structural reorganization and that the series of peaks on the curve are not due to measurement error, but to a sequence of non-catastrophic crazes spanned by fibrils that prevent further damage growth in the region.[12]

Fewer drop/rise events in the stress–time profiles of a membrane would indicate less non-catastrophic deformations and could result in better fuel cell performance under operating conditions. These results agree with the stress-strain test and indicate that the MB(HPPS-sDCDPS)_917, MB(HPPS-BP)_784 and R(HPPS-BP)_1260 samples have greater resistance to mechanical deformation at high temperature and humidity; however, they all showed overall lower conductivities compared to R(sDCDPS-BP)_654 and MB(HPPS-sDCDPS)_595. There is generally a trade-off between conductivity and mechanical durability, unless a near-perfect morphology could be achieved that would imbibe water without suffering big mechanical deformations, especially at high temperatures. In our case, sample MB(HPPS-sDCDPS)_595 would, *to some extent*, be

considered an *acceptable* balance between mechanical durability and conductivity. This sample showed high modulus and acceptable strain and stress at break compared with other samples having high conductivities. Constrained MEAs in fuel cells are subjected to local stresses generated by variations in humidity and temperature, creating a complex distribution of water that differs throughout the membrane.

Reduced mechanical modulus and reduced ductility would not only contribute to the initiation and propagation of damage zones but also generate fuel crossover pathways that accelerate chemical degradation. Apart from membrane chemical degradation, fuel crossover also reduces fuel cell efficiency due to voltage loss. For the MB(HPPS-sDCDPS)_595 membrane, ductility would increase if we can achieve higher molecular weight; this is a subject of our current work.

Physical degradation associated with humidity and temperature variations within the fuel cell during operation opens new fuel crossover pathways and contributes synergistically with chemical degradation to membrane degradation. The combined effect of physical and chemical degradation influences the rate and mode of membrane failure. Thus, for long term membrane survival and efficient fuel utilization, the membranes require modification to withstand internal stresses due to humidity and temperature changes. sPAES seem to be good candidates for long-term fuel cell usage based on these conditions, but conductivity needs to be improved.

In conclusion, internal reinforcement shown by some sPAES membranes would reduce the formation of radical species by reducing fuel crossover and cause a sharing of physical stresses which would prevent membrane failure and formation of crossover pathways.

Mechanical Creep Test. We performed mechanical tests to compare the mechanical durability of the various samples listed in Table 4, at operating fuel cells conditions. These tests reveal the importance of membrane mechanical properties and correlate how deterioration in mechanical properties results in chemical degradation that can lead to failure initiation in these membranes.

Constrained MEAs in fuel cells are subjected to local stresses generated by variations in humidity and temperature, creating a complex distribution of water that differs throughout the membrane. Nonetheless, in the interest of rapid membrane screening, creep tests were performed using a RH-TA Q800 dynamic mechanical analyzer to ascertain how membranes respond to a constant load in tension. The machine is equipped a relative humidity (RH) unit which allow for performing DMA tests at variable humidities from 0 to 95% and within temperature range of 25 to 95°C. Samples, after being equilibrated at 80°C and specified humidity for 60 min, were subjected to a constant specified value of stress for 3 h. The resulting strain was monitored during and after (release) application of stress for 3 h in each case. Figure 9 shows creep responses for the several sample listed in Table 4 (chemical structures shown in Figure 4), and tested under fuel cell operating conditions. Testing conditions of 80°C, 90% RH and under 10 MPa of constant stress represent very harsh conditions in terms of the mechanical durability of fuel cell membranes.

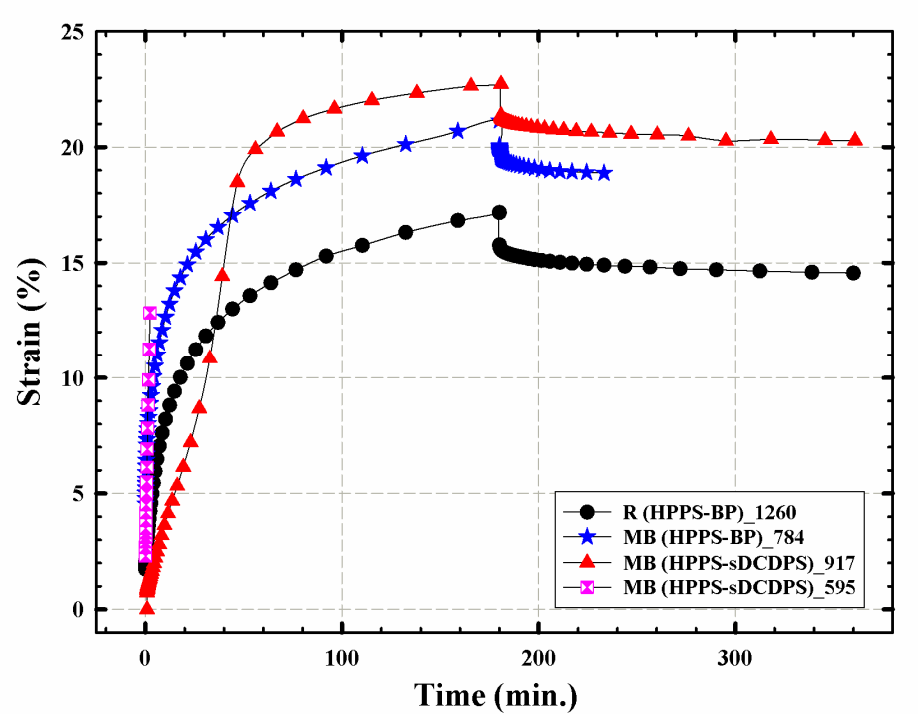

Figure 9. Tensile creep curves at 80°C, 90% RH and 10 MPa of constant stress for selected samples listed in Table 4.

Figure 9 shows that sample MB (HPPS_sDCDPS)_595 broke very early under the specified testing conditions. R(sDCDPS-BP)_654 also broke very early, but it is not shown in Figure 9. Conductivities of these two membranes were the highest among all samples.

Strain values observed for other sPAES samples in Figure 9 suggest greater stiffness from the perspective of creep and correlate with the high modulus values shown in the tensile test. The three sPAES membranes, other than MB (HPPS_sDCDPS)_595, showed much greater dimensional stability when compared to a Nafion® sample previously reported ("control" Nafion® sample in Ref. 12). The Nafion® sample yielded quickly at high RH% and high stress. Even with a reduction in RH and applied stress (test was conducted at 80°C, 50% RH and 5 MPa of constant stress), the Nafion® sample still yielded very early during the experiment and reached a plateau at a very high strain % value ≅ 225%. This suggests that yielding of Nafion® would be a result of conducting the test at 80°C, which is much higher than its T_g, thought to be around -20° C, plus the effect of water plasticization even at 50% RH. Meanwhile, sPAES samples showed a much lower strain % change, ≅ 15-24%, at twice the applied stress and %RH (10 MPa and 90% RH). This result suggests greater dimensional stability for sPAES samples under fuel cell operating conditions and high applied stress.

For samples MB (HPPS_sDCDPS)_595 and R(sDCDPS-BP)_654, the applied stress has to be reduced from 10 MPa to 1 MPa at 80° C and 90% to obtain a typical creep/recovery curves, as shown in Figure 10.

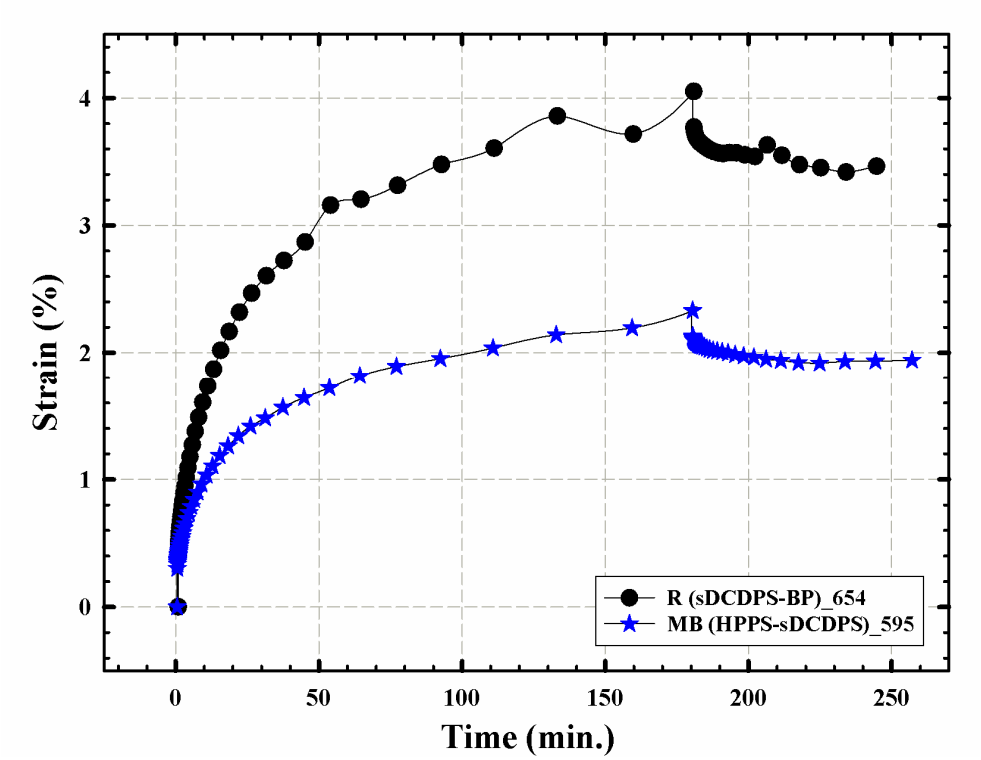

Figure 10. Tensile creep curves for the MB (HPPS_sDCDPS)_595 and R(sDCDPS-BP)_654 membranes at 80°C and 90 RH% and subjected to a reduced stress of 1 MPa.

To better understand the tensile creep behavior of the sPAES membranes shown in Figures 9 and 10, equilibrium water uptake measurements were conducted for the samples at 80°C using a TA Q5000SA moisture analyzer. Samples were subjected to a drying step for 100 min, and then a fixed humidity of 90% RH was applied for 3h. Water absorption curves for membranes with different compositions at fixed humidity and temperature are shown in Figure 11.

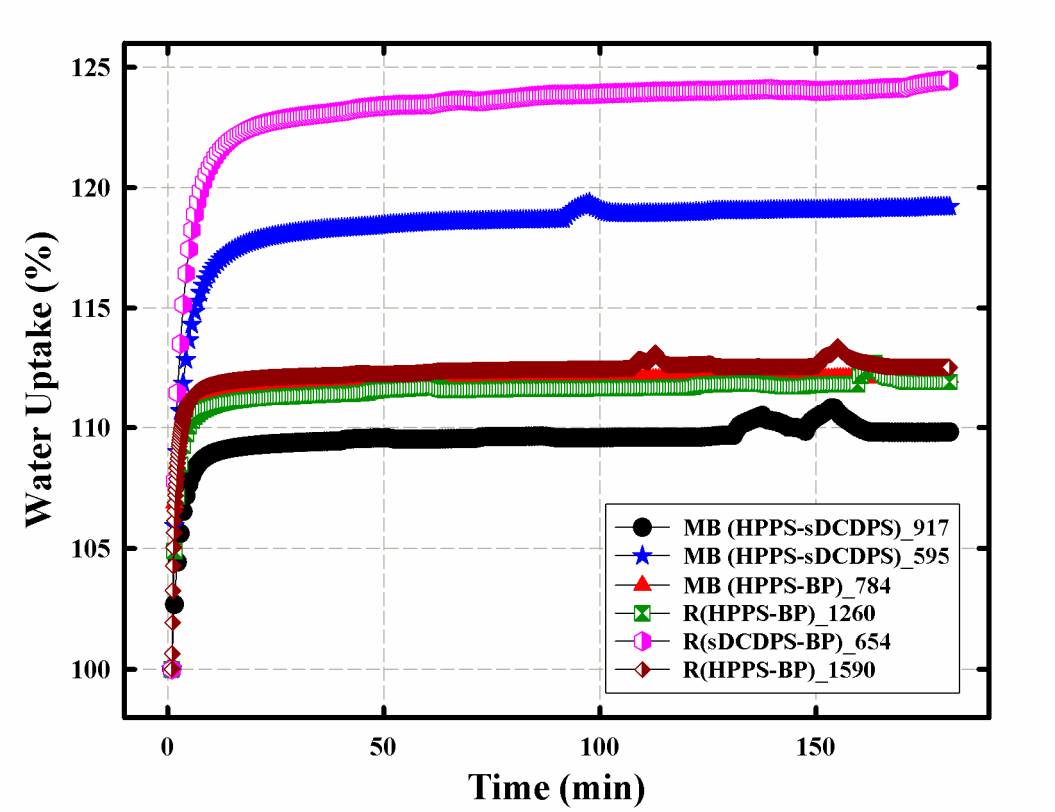

Figure 11. Water uptake change vs. time at 80°C and fixed humidity of 90% RH for sPAES samples with different compositions.

In Figure 11, samples MB (HPPS_sDCDPS)_595 and R(sDCDPS-BP)_654 showed the highest equilibrium water uptake at 80°C and 90% RH compared to all other samples. This explains the poor tensile creep performance under the same conditions for these samples as explained earlier. In terms of balance of mechanical durability and conductivity under test conditions outlined earlier, sample MB(HPPS-BP)_784 is considered to be the best. It is expected that improvements in the synthesis of these MBs, such as improved molecular weight and block length, would lead to further enhancement of their conductivity and mechanical strength, which is a subject of current work.

Physical degradation associated with humidity and temperature variations in fuel cells during operation opens new fuel crossover pathways and contributes synergistically with chemical degradation to membrane degradation. The combined effect of physical and chemical degradation influences the rate and mode of membrane failure. Thus, for long term membrane survival and efficient fuel utilization, the membranes require modification to withstand internal stresses due to humidity and temperature changes. The PAES-based materials studied in this project seem to be good candidates for long-term fuel cell usage based on these conditions, but with a required effort to increase their conductivity.

In conclusion, Nafion® does not have the high glass transition temperature characteristic of rigid chain aromatic-based sPAES hydrocarbon fuel cell membranes. Internal reinforcement shown by sPAES would reduce the formation of radical species by

reducing fuel crossover and cause a sharing of physical stresses which would prevent membrane failure and formation of crossover pathways.

Subtask 4.2 MEA Fabrication

Nafion. The following representative procedure for MEA fabrication from Nafion membranes has been published.[12] It is a decal transfer-type process.

Nafion® NRE 212 membranes obtained from E.I. DuPont Co. were cleaned by boiling in 8M nitric acid for 2 h followed by twice boiling in de-ionized water for 2 h to leach out residuals. The membranes were then dried at 80 ◦C under vacuum for 24 h.

MEAs were prepared using Pt/C catalyst for both anode and cathode. Catalyst ink was prepared by mixing 30% HP Pt on Vulcan XC-72 (BASF Fuel Cell Inc.) with a 5 wt% Nafion® solution in a homogenizer for 10 min. The targeted Nafion® content in the electrode was 30%. The ink was then applied on a Teflon® sheet by screen printing. This was then decal transferred onto the membrane in a Carver hot press at 120°C at a pressure of 13 atm for 5 min. Platinum loading in the electrode was gravimetrically estimated to be 0.41 ± 0.01 $mg \cdot cm^{-2}$. To compare degraded with non-degraded membranes, a control Nafion® MEA was fabricated using Vulcan XC-72 carbon black. The control MEA was subjected to identical ink making and decal transfer process but was not assembled in a fuel cell.

Hydrocarbon. MEAs from hydrocarbon membranes were produced by spraying rather than decal transfer; the ink was prepared in the same way outlined above for the Nafion benchmark membrane. MEAs were prepared by directly spraying successive layers of catalyst ink onto either side of a membrane. An infrared lamp was used to dry the MEA before application of each successive layer. A Teflon® mask was used to maintain a 5 cm^2 MEA active area during catalyst spraying. Platinum loading in the electrode was gravimetrically estimated to be 0.52±0.13mg/cm^2.

To compare degraded with non-degraded membranes for the sample R(HPPS-BP)_1,590, a control MEA was fabricated using the same procedure above and was subjected to identical catalyst ink spraying process but was not assembled in a fuel cell.

Task 5.0 Inorganic Sol-Gel Modification and Characterization of Nanocomposite Membranes

Nafion®. To improve durability of Nafion® membranes, samples were modified via an in situ sol-gel polymerization of titanium isopropoxide to generate titania quasi-networks in the polar domains.[1] The incorporated titania reduced water uptake but equivalent weight was essentially unchanged. Fuel cell performance of the modified membrane was inferior to that of the unfilled membrane although these were considered as model studies with focus on mechanical durability. Mechanical analysis of contractile stress buildup during drying from a swollen state in samples clamped at constant length demonstrated considerable reinforcement of Nafion® by the titania structures. Tensile studies showed that at 80°C and 100% relative humidity the dimensional change of the composite membrane was one half and the initial modulus was three times higher than that of the unmodified membrane. During an open circuit voltage decay test the voltage decay rate for the modified membrane was 3.5 times lower than that of control Nafion®. Fluoride emission for the composite was at least an order of magnitude lower than that of

the control Nafion® membrane indicating reduced chemical degradation. These model studies indicated that in situ inorganic modification offers a way to enhance fuel cell membrane durability by reducing both physical and chemical degradation.

In a follow-up study,[13] FTIR spectroscopy showed successful intraparticle chemical bond formation with incomplete condensation of TiOH groups. Although such modification can lower membrane fuel cell performance, this study was aimed at reducing membrane degradation without significantly altering performance in the sense of material optimization. The incorporated particles did not change membrane equivalent weight and the water uptake was similar to that of the unmodified Nafion® membrane. Membrane dimensional stability, mechanical properties, and ability to withstand contractile stresses associated with humidity change at 80°C and 100% RH were improved. An open circuit voltage (OCV) accelerated degradation test showed the titania modification held voltage better than the unmodified membrane. Performance deterioration of Nafion® after the OCV test was much higher than that of the modified membrane and the fluoride emission of the latter was lower. The degraded Nafion® membrane failed when subjected to creep; whereas the modified membrane remained intact with significantly low deformation. This study showed that inorganic modification offers a simple way to enhance membrane durability by reducing both physical and chemical degradation.

Hydrocarbon. This work was discontinued due to disappointing conductivity results and embrittlement of films resulting in poor handling properties.

Task 6.0 Fuel Cell Performance and Membrane Durability Studies

Nafion®. The mechanical properties of Nafion® membranes that were degraded after periods of OCV conditions in a fuel cell were studied.[12] Severe decreases in membrane modulus and ductility at 80°C and 100% relative humidity were observed. Stress-at-break values for 45 and 72 h degraded membrane–electrode assemblies (MEAs) were 6 and 9 times lower, respectively, while strain-at-break was 24 and 28 times lower, respectively, than that of a control MEA. Contractile stresses developed in constrained hydrated membranes that were then dried were conducted as a function of drying time. A pre-OCV degraded MEA, when subjected to creep deformation at 10 MPa, showed surface cracks which were not present in the control MEA. The 72 h-degraded MEA exhibited wider cracks than those of the 45 h degraded MEA sample. Spectroscopic analysis of degraded membranes showed various small molecule fragments associated with side chain degradation.

Hydrocarbon. MEAs were assembled in 5 cm^2 fuel cell hardware containing serpentine flow fields (Fuel Cell Technologies Inc.). Two 275 μm thick Toray carbon papers (TGPH-090) were used as gas diffusion layers in the assembly. It was sealed using two 225 μm thick Teflon gaskets, and torque of 4.5 N-m was applied on all bolts of the assembly. All MEAs were tested using a Scribner Associates Inc. model 850e fuel cell test station.

MEA performance was evaluated by generating voltage *vs*. current density curves in fuel cells at 80°C and 75% or 100% inlet RH. At the anode, pure H_2 was used as fuel and at the cathode, pure O_2 was used as the oxidant. The reactants flow rates were maintained at the rate of 200 mL/min. The current was scanned in 0.05 A increments

from a value of 0 A to its value at the point when the cell voltage dropped below 0.2 V. For each current density, the cell voltage was recorded after s 2 min holding time. Before obtaining polarization curves, the membranes were conditioned for 2 h at 0.9 V.

Figure 12 shows fuel cell polarization curves at 80°C and different RH% for a sample R(HPPS-BP)_1,590. Membrane internal resistance loss was high and the performance was poor compared to that of a Nafion membrane[13] under the same conditions, which could be due to inadequate hydration. Considering the lower water uptake (Figure 11) and lower proton conductivity of this PAES sample (1.4 mS/cm at 100% RH), its performance curve was expected to be low. The cell voltage significantly decreased with increasing load current density resulting in a very low maximum total cell power output of 0.35 W.

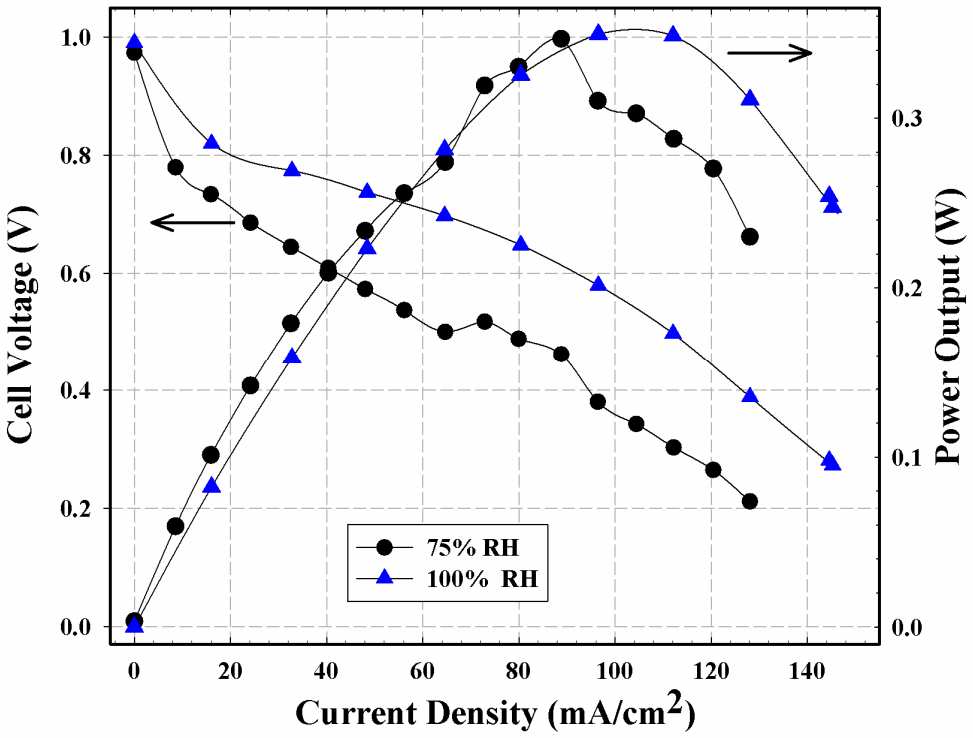

Figure 12. Cell voltage vs. current density and power curves for PAES, R(HPPS-BP)_1,590, membrane at 80°C and different RH%.

Polarization curves are typically split into three divisions: activation polarization, ohmic polarization, and concentration polarization. The OCV is the cell voltage when the current is zero. As the current begins to flow, the voltage drops due to the activation polarization. The OCV correlates with the crossover of hydrogen through the MEA. The polarization curve then takes on the linear shape associated with the ohmic losses, and this region can be correlated to the conductivity (or resistance) of the MEA. High tortuosity of H^+ pathways through the membrane due to isolated hydrophilic domains could be responsible for the resulting poor performance of the membrane. Performance slightly improved as the humidity increased from 75 to 100% RH. At high current densities, restrictions to the flow of reactants to the reaction sites lead to limiting current

density. Perhaps, the limited performance of this PAES membrane to such low current density makes it a suitable candidate for direct methanol rather than hydrogen fuel cells.

Open circuit voltage (OCV) decay test. Poor physical-chemical durability causes significant losses in fuel cell efficiency and operating lifetime. Inside the cell a membrane swells/shrinks with relative humidity increase/decrease. Cyclic compressive and contractile stresses eventually lead to craze and pinhole formation in local mechanically weak regions. This, in turn, generates pathways for H_2 and O_2 gas crossover and attack of radicals issuing from the decomposition of generated peroxide.[14,15,16] The macroscopic properties of Young's modulus, yield strength, and strain-at-break for Nafion® are reduced under hydrated conditions.[17] Open circuit voltage (OCV) tests are carried out in fuel cells at high temperature and low RH conditions which accelerate degradation. In addition to having high proton conductivity, it is necessary to eliminate or reduce membrane fuel crossover without affecting fuel cell performance. Internal reinforcement, through rigid hydrocarbon backbone, should reduce H_2 fuel crossover by limiting membrane swelling and introduce obstacles that increase gas transport tortuosity. On the other hand, this backbone also introduces proton migration tortuosity that might reduce proton conductivity. Thus, performance optimization becomes a trade-off between high conductivity and good membrane durability.

The accelerated degradation test was performed to test the PAES membrane durability at high temperature and low RH conditions. MEAs were tested under OCV conditions at 90°C and 30% inlet gases RH. At the cathode, O_2 was used as oxidant and at the anode H_2 was used as the fuel with gas flow maintained at the rate of 200 mL/min. The test was performed for 62 h for the PAES and for 48h for the Nafion 112 control sample.

The voltage curves for two membranes subjected to OCV testing are shown in Figure 13. One reason why the OCV drops with time is increasing fuel crossover. Gases not consumed diffuse to the opposite side of the membrane. This not only reduces the OCV but also generates hydrogen peroxide, which on decomposition attacks the membrane and thus reduces its molecular weight. Under the combined effects of physical and chemical degradation, defects such as uneven thickness and micro-cracks grow, promoting diffusion of more gas and further reduction of OCV. This auto-accelerating process continues until membranes fail due to large pinhole formation. The extent of membrane degradation scales with OCV test time with the degraded MEAs displaying reduced mechanical properties as compared to the control MEA. The cell voltage in the case of Nafion apparently drops very quickly compared to PAES, especially in the first 30h. This could be due to increase in gas diffusion resulted from the formation of cracks or pores.

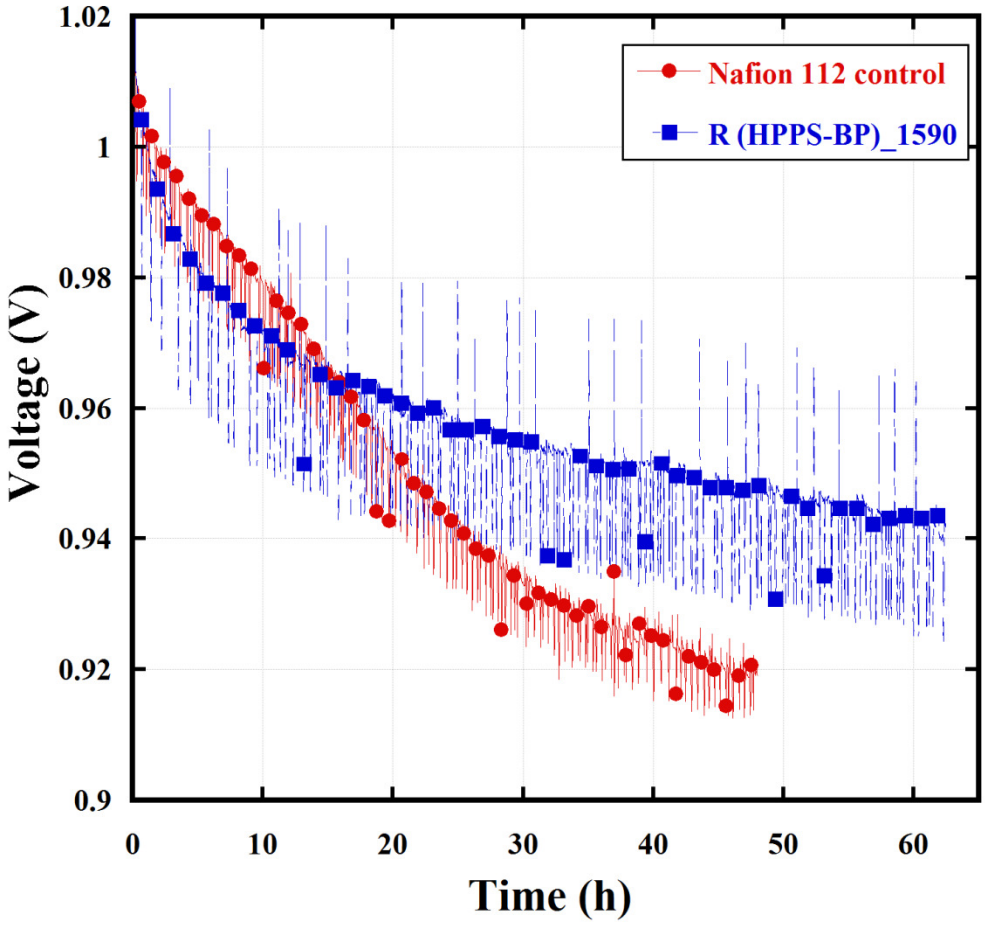

Figure 13. OCV curves for PAES, R(HPPS-BP)_1,590, and Nafion membranes at 90°C and 30% RH.

After 48h, the voltage drop had become linear for both Nafion and R(HPPS-BP)_1,590 samples (Figure 13). Total loss for the Nafion sample was 0.09 V at an average rate of 1.9 mV/h; whereas, R(HPPS-BP)_1,590 lost only 0.055 V at an average rate of 1.12 mV/h. Throughout the latter course of the experiment, OCV for the PAES not only stayed higher but also decayed at a much lower rate, which is attributed to better dimensional stability and improved mechanical and gas barrier properties. PAES's rigid backbone reinforcement adds gas diffusion tortuosity that restricts membrane degradation and OCV loss due to reduced fuel crossover.

Figure 14 shows fuel cell performance curves for R(HPPS-BP)_1,590 before and after 62 h in the OCV test, at 80°C and 75% or 100% inlet RH. The performance of the membrane slightly decreased after the OCV test. Nafion was reported[1] to have higher performance deterioration post-OCV degradation due to increased fuel crossover due to high membrane degradation. The inability of Nafion to withstand physical stresses severely degraded the membrane and pathways for fuel crossover were created. This not only degrades the Nafion membrane faster, reducing the life of the fuel cell but also makes it less efficient due to the voltage penalty associated with fuel crossover.[13]

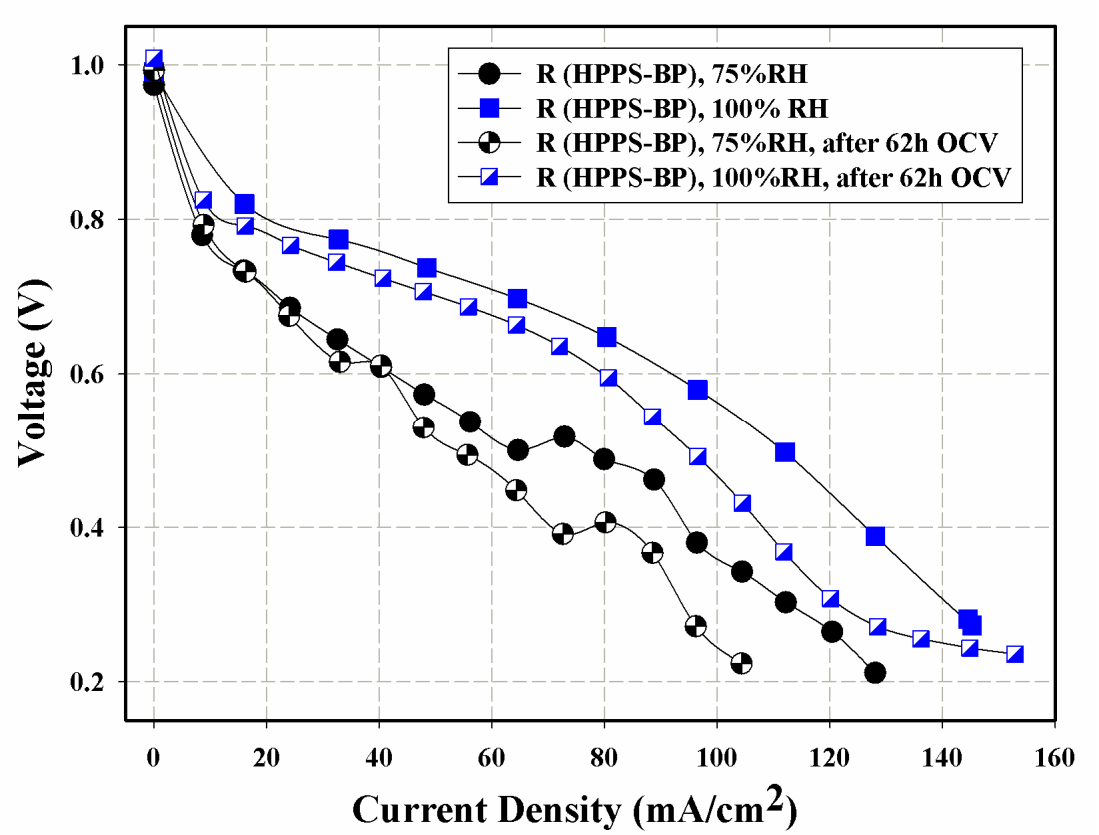

Figure 14. Fuel cell voltage vs. current density for sample R(HPPS-BP)_1,590 before and after OCV for 62h at 90°C and 30% RH.

Mechanical properties of OCV-degraded membranes. Tensile properties under typical fuel cell operating conditions were measured, after OCV degradation test, in an environmental chamber equipped with a sparger to supply a humidified nitrogen stream. The membranes, after being clamped in the chamber, were conditioned for 2 h with a 100% RH nitrogen stream at a flow rate of 300 mL/min and a temperature of 80°C. Samples were then stretched at a rate of 10 mm/min. Figure 15 shows stress vs. strain curves for control and 62h-degraded MEAs of the R(HPPS-BP)_1,590 sample. The failure of degraded MEAs at low strain indicates reduced ductility post-degradation. Both strain-at-break and stress-at-break are lower for the degraded samples than for the control MEA, presumably due to decreased molecular weight caused by chemical degradation. Figure 16 shows expanded initial curve regions for the same runs. The curves are displaced rightward along the strain axis because of dimensional increase due to water uptake. After this stress lag, the curves are 'typical' and a modulus can be computed from the initial, displaced linear regions.

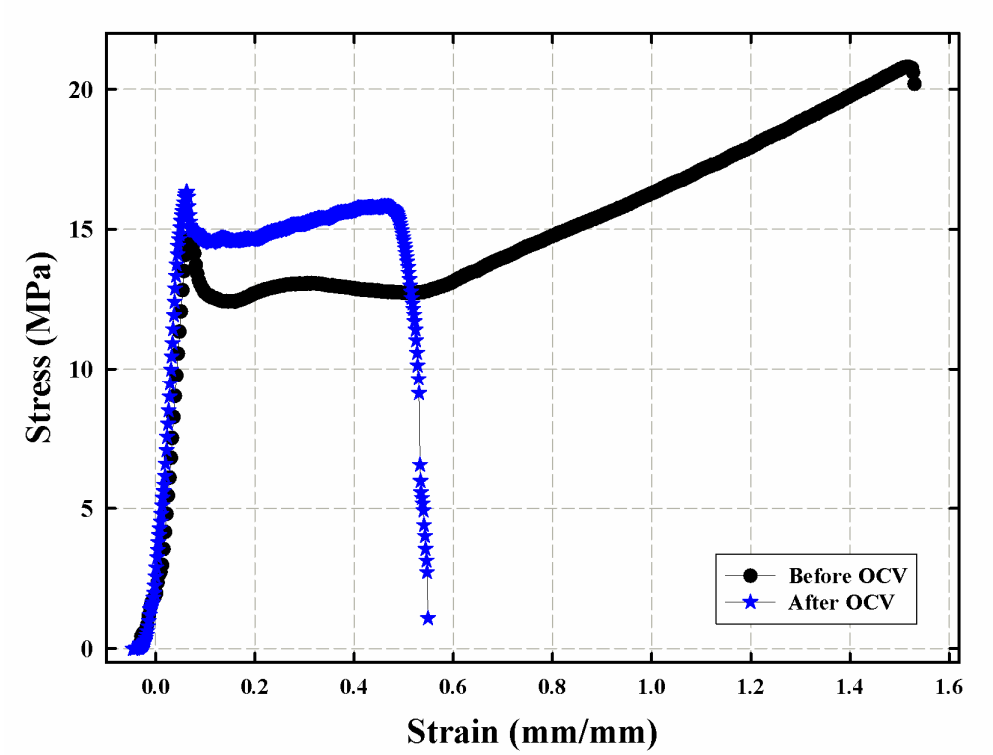

Figure 15. Stress-strain curves at 100% RH and 80°C for PAES sample, R(HPPS-BP)_1,590, before and after 62h OCV degradation test.

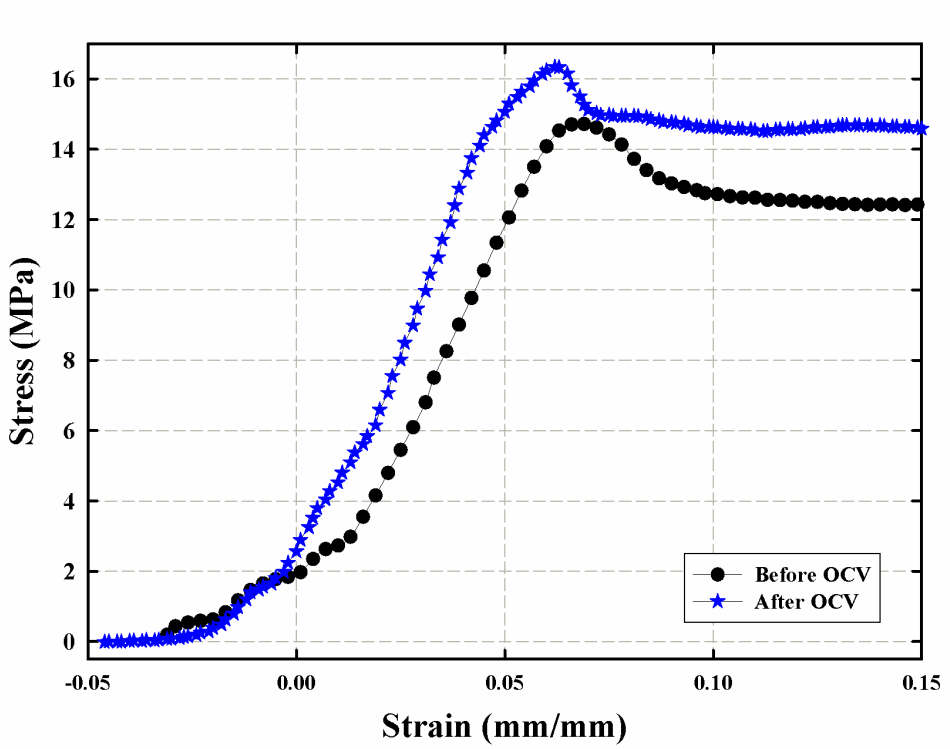

Figure 16. Initial portion of the stress-strain curves at 100% RH and 80°C for PAES sample, R(HPPS-BP)_1,590, before and after 62h OCV degradation test.

The modulus and the yield stress were higher for the degraded MEA. The modulus was 224 and 326 MPa before and after OCV, respectively. This indicates that the membrane can still withstand stresses, is less likely to yield, and can survive longer in the fuel cell even after 62h of degradation. Strain-at-break and stress-at-break, however, were lower as expected due to degradation to the sample. Shortened chains can easily slip through entanglements and thus are unable to resist deformation. In general, a reduction of the modulus suggests that sample can easily deform when subjected to stresses and rupture due to reduced stress and strain-at-break, thereby promoting pathways for fuel crossover that lead to membrane failure.

Contractile stresses, generated by the membranes as they attempted to shrink when subjected to a drop in RH, were monitored. In this test, samples were held at their extended swollen length by slowly adjusting the crosshead position until a tension of 0.4N was reached. The crosshead position was then locked, and the 100% RH nitrogen stream was switched to dry nitrogen at the same flow rate while maintaining the temperature of the dry stream and chamber temperature at 80°C. The ensuing contractile force was then monitored as a function of time. The stress levels developed are diagnostic of the ability of the membrane to resist dimensional changes associated with drying and related to mechanical durability. Figure 17 shows contractile stresses developed for the control and 62 h-degraded MEAs measured over a time span of 2 h after the RH drop.

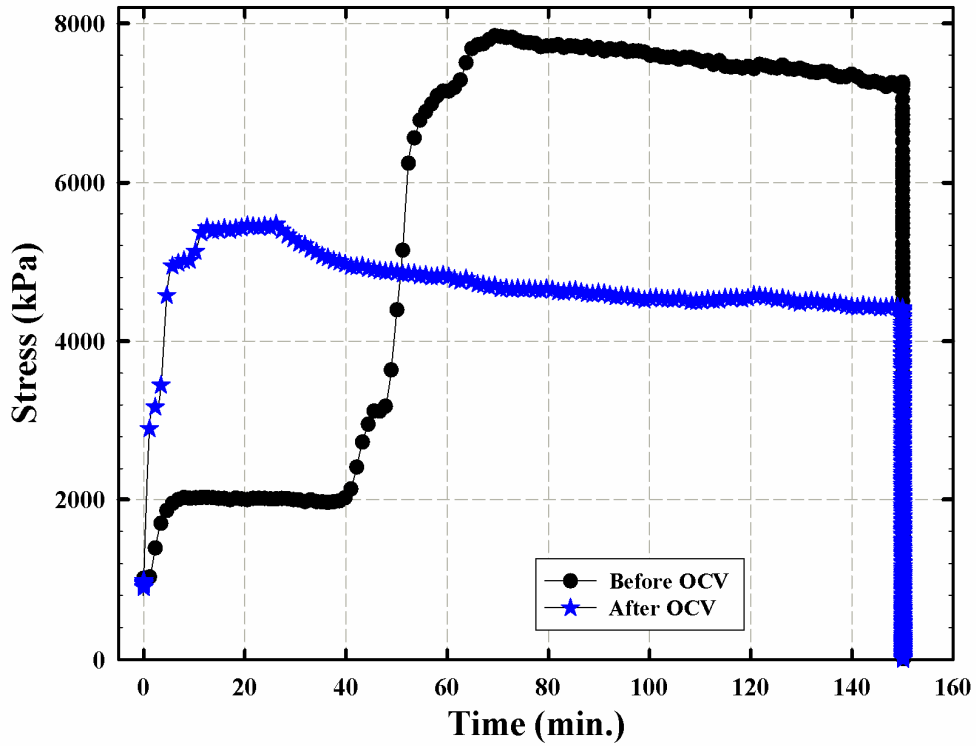

Figure 17. Contractile stress response to humidity decrease from 100 to 0% RH at 80°C for R(HPPS-BP)_1,590 MEA before and after 62h OCV degradation test.

The stress–time profiles for all MEAs, before and after OCV, peak at different times with the control exhibiting higher stress than that of the degraded membranes. None of the samples could withstand the induced contractile stress and eventually yielded, most likely due to macromolecular chain slippage through entanglements. These entanglements will be fewer and less effective as the average molecular weight is reduced by chemical degradation, thereby accounting for the drop in peak stress for the degraded materials. The degraded sample showed a very early initial stress increase; whereas the control sample showed stress increase in two steps, with the second step occurring 40 min after the start. The second step increase could be due to a longer range structural reorganization, the origin of which is not clear to us at this point. Increases in stress for different MEAs are believed to be not due to measurement error, but to a sequence of non-catastrophic crazes spanned by fibrils that prevent further damage growth in the region.[12] The control and degraded MEAs seem to possess enough ductility to enable them to deform and maintain their structural integrity. The degraded MEA was able to withstand stress, ≅ 5500 kPa, even after 62h of OCV degradation.

Creep tests were performed using a RH-TA Q800 dynamic mechanical analyzer to ascertain how MEA films respond to a constant load in tension. The instrument is equipped with a relative humidity (RH) unit which allows for performing DMA tests at variable humidities from 0 to 95% and within a temperature range of 25 to 95°C. Samples, after being equilibrated at 80°C and specified humidity for 60 min, were subjected to a constant specified value of stress for 3 h. The resulting strain was monitored during and after (release) application of stress for 3 h in each case.

Figure 18 shows creep response for the control and 62 h-degraded MEAs measured under fuel cell operating conditions. Testing conditions of 80°C, 90% RH and under 10 MPa of constant stress represent very harsh conditions in terms of the mechanical durability of fuel cell membranes. The degraded MEA deformed by 140%, of which 7% was recovered after stress removal. The control MEA film deformed by 80%, of which 9% was recovered after stress removal. We believe that the second decay in strain at 250 min is an experimental artifact and could be due to sample slippage. After degradation, due to reduced ductility, the applied stress may generate microscopic cavities rather than crazes that are spanned by fibrils.[13] Higher strain observed for degraded MEAs relative to the control MEA is quite interesting as it resembles the behavior of high molecular weight glassy polymers. This behavior indicates the membrane became less brittle and tougher upon degradation. The membrane undergoes chain slippage associated with large scale deformation in high molecular weight polymers upon deformation rather than local rupture in order to relieve applied stress. However, the higher strain observed for degraded MEAs relative to the control MEA does not seem, at first thought, to correlate with the higher modulus of degraded samples, as this would indicate smaller stiffness from the perspective of creep. A complete understanding of this result is not clear to us at the moment. The strain recovery % of the degraded and control samples is almost the same which suggests the absence of weak spots which would facilitate gas crossover.

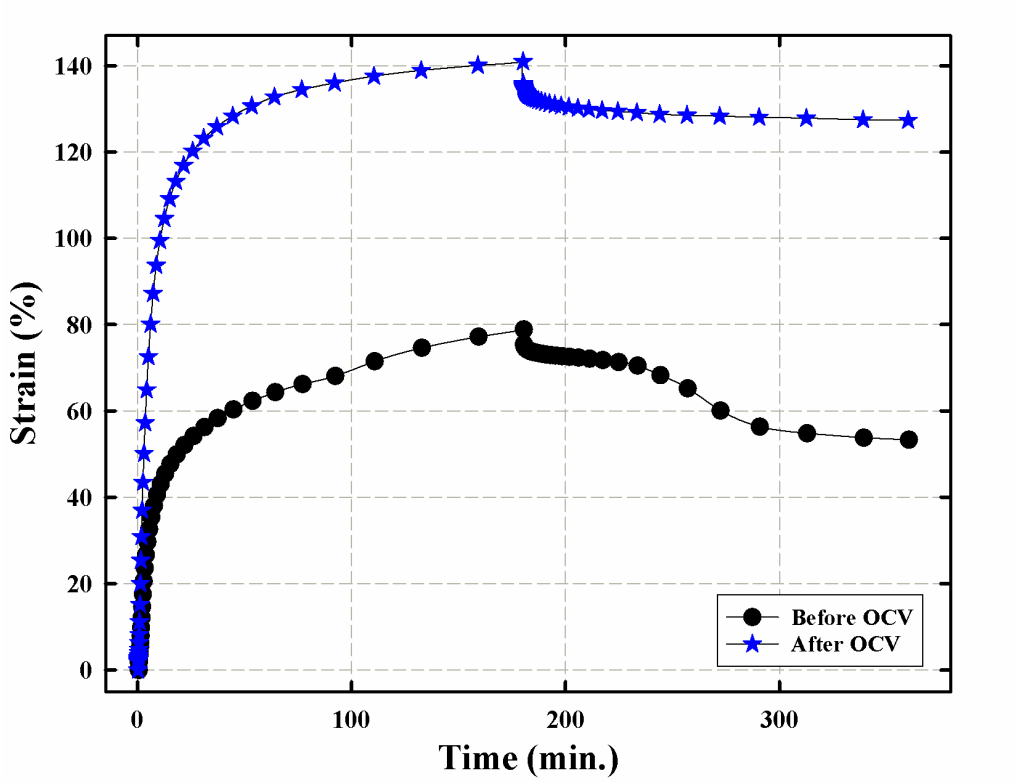

Figure 18. Tensile creep curves at 80°C, 90% RH and under 10 MPa of constant stress for PAES MEA, R(HPPS-BP)_1,590, before and after 62h OCV degradation test.

The overall results of creep, contractile stress, and mechanical tensile tests support the conclusion that degraded MEAs of PAES membranes can handle stress and are more likely to be more durable in a fuel cell, even after subjected to 62h of OCV degradation. Degraded Nafion MEAs were reported[1] to be unable to withstand stresses, possess reduced ductility and poorer mechanical properties, and start to form cracks after 45h of OCV degradation. Physical degradation of Nafion associated with humidity and temperature variations in the cell open new fuel crossover pathways and contribute synergistically with chemical degradation to membrane degradation.[1] Thus, for long term Nafion membrane survival in a fuel cell, physical or chemical reinforcement is needed because it does not have the high glass transition temperature characteristic of rigid chain aromatic-based hydrocarbon membranes like PAES. Internal reinforcement of PAES aromatic backbone lowers the formation of radical species by reducing fuel crossover and cause a sharing of physical stresses which would prevent membrane failure and formation of crossover pathways.

Task 7.0 Project Management and Reporting

Reports and other deliverables have been provided in accordance with instructions in the Federal Assistance Reporting Checklist. Project reporting has included 1) participation in the annual DOE Hydrogen Program Review; 2) participation in Tech Team meetings, as requested by DOE; and 3) preparation and presentation of detailed

briefings of plans, progress, and results of the technical effort to DOE personnel when requested.

Milestones

Y1, Q4 - Establish in-house benchmark data on Nafion and inorganically modified Nafion for all critical property characterization tests, under the same conditions as those to be performed for the experimental aromatic hydrocarbon membranes.
Status: Complete.
Y2, Q4 - Establish baseline data for all critical properties and microstructure of the hydrocarbon membranes to identify promising membrane candidates for fuel cell evaluations.
Status: Block copolymers with hydrophilic blocks consisting of both HPPS and 3,3′-disulfonate-4,4′-diclorodiphenylsulfone appear to be promising. Structural characterization and membrane durability investigations are underway. Pendant N-heterocycle aromatic main-chain polymers and PFPO-based block copolymers have been eliminated from consideration at this time.
Y3, Q2 - Demonstrate that critical membrane properties, fuel cell performance and accelerated degradation (both mechanical and chemical durability) of one or more MEAs from the three separate synthesis approaches has improved relative to the baseline materials, under Tasks 3 and 4, and meets the DOE 2010 MEA targets.
Status: The *ex-situ* durability properties and conductivity of sPAES multi-block copolymers containing HPPS and sDCDPS in the hydrophilic block show sufficient promise to warrant MEA fabrication. Efforts are underway to produce additional quantities of materials to produce MEAs. Fuel cell performance and accelerated *in-situ* OCV degradation tests were conducted on sPAES multi-block copolymers membrane films. They showed promising results regarding their mechanical durability even after 62h of OCV degradation. Further improvement in membrane fuel cell performance is still needed enhancing the conductivity at high temperature.

TECHNOLOGY TRANSFER ACTIVITIES

Publications

1. Hassan, M.K; Mauritz, K.A. “Broadband Dielectric Spectroscopic Studies of Annealed Nafion® Membranes” *ECS Transactions* **2009**, *25*(1), 371-384.
2. Chen, H.; Mauritz, K.A. “Proton Conducting Sulfonated Poly(styrene-b-ethylene/butylene-b-styrene)/silicated Nanocomposite Membranes as Models for Polymer Electrolyte Membranes” *ACS Div. Polym. Chem., Polym. Preprs.* **2009**, *50*(1), 283-284.
3. Patil, Y.P.; Mauritz, K.A. “Effect of Accelerated Fuel Cell Degradation on Mechanical Properties of Nafion® Membranes” *Polym. Mat. Sci. Eng.* **2009**, *101,* 969-970.
4. Patil, Y.P.; Kulkarni, S.; Mauritz, K.A. “Effect of in-situ Grown Titania Particles on the Performance and Durability of Nafion® Membranes” *Prep, Pap.-Am. Chem. Soc., Div. Fuel Chem.* **2009**, *54*(2), xxxx.

5. Nalawade, A.; Mauritz, K.A. "Generation of silica composition profiles in Nafion® membranes via in situ sol-gel reactions and hybrid membrane fuel cell performance" *Prepr. Pap.-Am. Chem. Soc., Div. Fuel Chem.* **2009**, *54*(2), xxxx.
6. Patil, Y.; Mauritz, K.A. "Durability Enhancement of Nafion® Fuel Cell Membranes Via In Situ Sol-Gel-Derived Titanium Dioxide Reinforcement" *J. Appl. Polym. Sci.* **2009**, *113*, 3269–3278.
7. Patil, Y.P.; Jarrett, W.L.; Mauritz, K.A. "Deterioration of Mechanical Properties: A Cause for Fuel Cell Membrane Failure" *J. Membrane Sci.* **2010**, *356*, 7–13.
8. Baranek, A.; Suggs, S.; Patton, D. "Synthesis of Tethered Triazole Poly(aryl ether sulfones) Toward High Temperature, Low Humidity Proton Exchange Membranes" *ACS Div. Polym. Chem., Polym. Preprs.* **2010**, *51*(1), 638-639.
9. Nalawade, A.; Hassan, M.K.; Mauritz, K.A.; Litt, M.H. "Broadband Dielectric Spectroscopy Studies of Instrument - in situ Annealed Poly (2,5- benzimidazole) Membrane Materials" *Prep. Pap. - Am. Chem. Soc., Div Fuel Chem.* **2010**, *55*(2), 243.
10. Kulkarni, S.; Mauritz, K.A. "Inorganic Sol-gel Modified Solution Cast Nafion Membranes for Optimum Performance and Durability in Fuel Cells" *Prep. Pap. - Am. Chem. Soc., Div Fuel Chem.* **2010**, *55*(2), 238
11. Patil, Y.; Kulkarni, S.; Mauritz, K.A. "In Situ Grown Titania Composition for Optimal Performance and Durability of Nafion® Fuel Cell Membranes" *J. Appl. Polym. Sci.* **2011**, *121*, 2344–2353.
12. Chen, H.; Hassan, M.K.; Peddini, S.K.; Mauritz, K.A. "Macromolecular Dynamics of sulfonated Poly(styrene-*b*-ethylene-*ran*-butylene-*b*-styrene) Block Copolymers by Broadband Dielectric Spectroscopy" *Eur. Polym. J.* **2011**, *47*, 1936-1948.
13. Hassan, M.K; Nalawade, A.; Abukmail, A.; Patil, Y.; Mauritz, K.A. "Analysis of Nafion® Fuel Cell Membrane Chemical Durability Using Broadband Dielectric Spectroscopy" *ECS Transactions* **2011**, *41*(1), 1359-1370.
14. Nalawade, A.; Abukmail, A.; Hassan, M.K.; Mauritz. K.A. "Sub-Tg Macromolecular Motions in Phosphoric Acid Doped Polybenzimidazole Membranes for High Temperature Fuel Cell Applications" *ECS Transactions* **2011**, *41*(1), 1449-1459.
15. Li, H.; Jackson, A.B.; Kirk, N.J.; Mauritz, K.A.; Storey, R.F. "Poly(arylene ether sulfone) Statistical Copolymers Bearing Perfluoroalkylsulfonic Acid Moieties" *Macromolecules* **2011**, *44*(4), 694–702.
16. Li, H.; Kirk, N.J.; Mauritz, K.A.; Storey, R.F. "Poly(arylene ether sulfone) Multi-Block Copolymers Bearing Perfluoroalkylsulfonic Acid Groups" *Polymer* **2011**, *52*(16), 3550-3559.
17. Hassan, M.K.; Nalawade, A.; Mauritz, K.A. "Analysis of Macromolecular and Proton Motions in Fuel Cell Membranes Using Dielectric Spectroscopy" *ACS Div. Polym. Chem., Polym. Preprs.* **2011**, *52*(1), 484-485.
18. Hassan, M.K.; Nalawade, A.; Mauritz, K.A. "Macromolecular and Proton Motions in Fuel Cell Membranes via Dielectric Spectroscopy" *Prep. Pap.-Am. Chem. Soc., Div. Fuel Chem.* **2011**, *56*(2), 220.

19. Kirk, N.J.; Mauritz, K.A. "Preparation and Characterization of a Multiblock Sulfonated Poly(arylene ether sulfone) for Proton Exchange Membranes" *Prep. Pap.-Am. Chem. Soc., Div. Fuel Chem.* **2011**, *56*(2), 250.
20. Baranek, A.D.; Suggs, S.A.; Patton, D.L. "Synthesis of Tethered Triazole Poly(aryl ether sulfone) Toward High Temperature, Low Humidity Proton Exchange Membranes" *ACS Div. Fuel Chem. Preprs.* **2011**, *56*(2), 537-538.
21. Hassan, M.K.; Abukmail, A.; Mauritz, K.A. "Broadband Dielectric Spectroscopic Studies of Molecular Motions in a Nafion® Membrane vs. Annealing Time and Temperature" *Eur. Polym. J.* **2012**, *48*, 789–802.
22. Nalawade, A.; Hassan, M.K.; Jarrett, W.A.; Mauritz, K.A.; Litt, M.H. "Broadband Dielectric Spectroscopy Studies of Glassy State Relaxations in Annealed Poly (2,5-benzimidazole)" *Polym. Int*. **2012**, *61*(1), 55-64.
23. Mauritz, K.A.; Nalawade, A.; Hassan, M.K. "Proton Exchange Membranes for H_2 Fuel Cells Applications" In *Sol-Gel Processing for Conventional and Alternative Energy*; Aparicio, M., Jitianu, A., Klein, L.C., Eds.; Springer: New York, 2012; Chap. 5, pp 73-98.

Presentations

1. Mauritz, K.A. "Polymer Membranes in Fuel Cells" Symposium Honoring Charles A. Wilkie on the Occasion of his Retirement, Marquette U., Milwaukee, WI, June 6, **2009**.
2. Chen, H.; Mauritz, K.A. "Proton Conducting Sulfonated Poly(styrene-b-ethylene/butylene-b-styrene)/silicated Nanocomposite Membranes as Models for Polymer Electrolyte Membranes" Poster, American Chemical Society National Meeting, Polymer Division, Salt Lake City, UT, March, **2009**.
3. Patil, Y.P.; Mauritz, K.A. "Effect of Accelerated Fuel Cell Degradation on Mechanical Properties of Nafion® Membranes" Poster, American Chemical Society 238th National Meeting, PMSE Division, Washington, DC, August, **2009**.
4. Patil, Y.P.; Kulkarni, S.; Mauritz, K.A. "Effect of in-situ Grown Titania Particles on the Performance and Durability of Nafion® Membranes" American Chemical Society National Meeting, Fuel Division, Washington, DC, August, **2009**.
5. Nalawade, A.; Mauritz, K.A. "Generation of silica composition profiles in Nafion® membranes via in situ sol-gel reactions and hybrid membrane fuel cell performance" Oral, American Chemical Society National Meeting, Fuel Division, Washington, DC, August, **2009**.
6. Mauritz, K.A.; Hassan, M.K.; Rhoades, D.W. "Characterization of Molecular Motions in Nafion® Fuel Cell Membranes by Dielectric Spectroscopy" 216th Electrochem. Soc. Meet., Vienna, Austria. October, **2009**.
7. Mauritz, K.A. "Characterization of Molecular Motions in Fuel Cell Membranes by Dielectric Spectroscopic Techniques" Chevron-Phillips Speaker, Macromol. Sci. Eng. Sem. Ser., Virginia Tech, Blacksburg, VA, Jan. 27, **2010**.
8. Baranek, A.; Suggs, S.; Patton, D. "Synthesis of Tethered Triazole Poly(aryl ether sulfones) Toward High Temperature, Low Humidity Proton Exchange Membranes" Poster, Waterborne Symposium, New Orleans, LA, February, **2010**.
9. Baranek, A.; Suggs, S.; Patton, D. "Synthesis of Tethered Triazole Poly(aryl ether sulfones) Toward High Temperature, Low Humidity Proton Exchange

Membranes" Poster, American Chemical Society National Meeting, Polymer Division, San Francisco, CA, **2010**.

10. Nalawade, A.; Hassan, M.K.; Mauritz, K.A.; Litt, M.H. "Broadband Dielectric Spectroscopy Studies of Instrument - in situ Annealed Poly (2,5- benzimidazole) Membrane Materials" Oral, American Chemical Society National Meeting, Fuel Division, Boston, MA, August **2010**.
11. Kulkarni, S.; Mauritz, K.A. "Inorganic Sol-gel Modified Solution Cast Nafion Membranes for Optimum Performance and Durability in Fuel Cells" Oral, American Chemical Society National Meeting, Fuel Division, Boston, MA, August **2010**.
12. Hassan, M.K.; Nalawade, A.; Mauritz, K.A. "Analysis of Macromolecular and Proton Motions in Fuel Cell Membranes Using Dielectric Spectroscopy" Oral, American Chemical Society National Meeting, POLY/PMSE Joint Session, Anaheim, CA, March **2011**.
13. Kirk, N.J.; Mauritz, K.A. "Preparation and Characterization of a Multiblock Sulfonated Poly(arylene ether sulfone) for Proton Exchange Membranes" Oral, American Chemical Society National Meeting, Fuel Division, Denver, CO, August **2011**.
14. Hassan, M.K.; Nalawade, A.; Mauritz, K.A. "Macromolecular and proton motions in fuel cell membranes via dielectric spectroscopy" Oral, American Chemical Society National Meeting, Fuel Division, Denver, CO, August **2011**.
15. Baranek, A.; Suggs, S.; Patton, D. "Synthesis of Tethered Triazole Poly(arylether sulfones) toward High Temperature, Low Humidity Proton Exchange Membranes" Poster, American Chemical Society National Meeting, Fuel Division, Denver, CO, August **2011**.
16. Baranek, A.D.; Narayanan, J.; Tyson, G.; Kendrick, L.; Patton, D.L. "Synthesis and Characterization of Cross-linked, Quaternary Ammonium Polybenzoxazines for Anion Exchange Membranes" Poster, Waterborne Symposium, New Orleans, LA, February, **2012**. (1st Place Best Poster Award)

REFERENCES

(1) Patil, Y.; Mauritz, K.A. *J. Appl. Polym. Sci.* **2009**, *113*, 3269-3278.
(2) Li, H.; Jackson, A.B.; Kirk, N.J.; Mauritz, K.A.; Storey, R.F. *Macromolecules* **2011**, *44*(4), 694–702.
(3) Li, H.; Kirk, N.J.; Mauritz, K.A.; Storey, R.F. *Polymer* **2011**, *52*(16), 3550-3559.
(4) Avram, E.; Butu, E.; Luca, C. *J.M.S.-Pure Appl. Chem.* **1997**, *A34*, 1701-1714.
(5) Einsla, B.R. Ph.D. Dissertation, Virginia Polytechnic Institute, **2005**.
(6) Mauritz, K.A.; Hassan, M.K. *ECS Transactions* **2009**, *25*(1), 371-384.
(7) Hassan, M.K; Nalawade, A.; Abukmail, A.; Patil, Y.; Mauritz, K.A. *ECS Transactions* **2011**, *41*(1), 1359-1370.
(8) Hassan, M.K.; Abukmail, A.; Mauritz, K.A. *Eur. Polym. J.* **2012**, *48*, 789-802.
(9) Patil, Y.P.; Seery, T.A.P.; Shaw, M.T.; Parnas, R.S. *Ind. Eng. Chem. Res.* **2005**, *44*, 6141–6147.

(10) Huang, X.; Solasi, R.; Zou, Y.; Feshler, M.; Reifsnider, K.; Condit, D.; Burlatsky, S.; Medden, T. *J. Polym. Sci., Part B: Polym. Phys.* **2006**, *44*, 2346–2357.
(11) Aoki, M.; Uchida, H.; Watanabe, M. *Electrochem. Commun.* **2005**, *7*, 1434–1438.
(12) Patil, Y.P.; Jarrett, W.L.; Mauritz, K.A. *J. Membrane Sci.* **2010**, *356*, 7–13.
(13) Patil, Y.; Kulkarni, S.; Mauritz, K.A. *J. Appl. Polym. Sci.* **2011**, *121*, 2344-2353.
(14) LaConti, A.B.; Hamdan, M.; McDonald, R.C. In *Handbook of Fuel Cells: Fundamentals, Technology, and Applications*; Vielstich, W., Lamm, A., Gasteiger, H., Eds.; John Wiley & Sons Ltd.: Chichester, England; **2003**.
(15) Crum, M.; Liu, W. *ECS Transactions* **2006**, *3*, 541-550.
(16) Kusoglu, A.; Karlsson, A.M.; Santare, M.H.; Cleghorn, S.; Johnson, W.B. *J. Power Sources* **2006**, *161*, 987-996.
(17) Tang, Y.; Karlsson, A.M.; Santare, M.H.; Gilbert, M.; Cleghorn, S.; Johnson, W.B. *Mat. Sci. Eng.: A* **2006**, *425*, 297-304.

Task Number	Project Milestones	Task Completion Date				Progress Notes
		Original Planned	Revised Planned	Actual	Percent Complete	
1.0	Acquisition of Equipment	6/30/09	6/30/10		100%	Complete
2.0	Synthesis of Polymers	1/31/10	5/31/2012		100%	Complete
2.1	Synthesis of Aromatic Polymers w/Tethered, Acidic Ion Exchange	1/31/10	5/31/2012		100%	Complete
2.2	Synthesis of Pendant N-heterocycle Aromatic Main-chain Polymers	1/31/10	12/31/11		80%	Discontinued
2.3	Synthesis and Phase Behavior of PFPO-based Block Copolymers	1/31/10	12/31/11		70%	Discontinued
3.0	Establishment of Standard Membrane Benchmark Data	3/31/09	5/31/12		N[1] 100% H[2] 100%	Complete Complete
Y1Q4	Benchmark Nafion		1/31/10		100%	Complete
4.0	Membrane Characterization and MEA Fabrication	1/31/10	5/31/2012		N[1] 100% H[2] 100%	Complete Complete
4.1	Membrane *ex situ* Durability Characterization	1/31/10	5/31/2012		N[1] 100% H[2] 100	Complete Complete
4.2	MEA Fabrication Development	1/31/10	5/31/2012		N[1] 100% H[2] 100%	Complete Complete
Y2Q4	Baseline Data Hydrocarbon Membranes		5/31/2012		H[2] 100%	Complete
5.0	Inorganic Sol-Gel Modification and Characterization of Nanocomposite Membranes	1/31/10	5/31/2012		N[1] 100% H[2] 55%	Complete Discontinued
6.0	Fuel Cell Performance and Membrane Durability Studies	1/31/10	5/31/2012		N[1] 100% H[2] 100%	Complete Complete
Y3Q2	Demonstrate synthesis approach improved relative to baseline materials		5/31/2012		H[2] 100%	Complete
7.0	Project Management and Reporting	1/31/10	5/31/2012		100%	Complete